LONGITUDINAL STABILITY AND CONTROL DERIVATIVES OBTAINED FROM FLIGHT DATA OF A PA-30 AIRCRAFT

FINAL REPORT

PRINCIPAL INVESTIGATORS

Dale R. Turley

Doral R. Sandlin

April, 1981

California Polytechnic State University

Aeronautical Engineering Department

San Luis Obispo, California

Grant No. NCC4-1

TABLE OF CONTENTS

LIST OF TABLES

LIST OF FIGURES

NOMENCLATURE

All of the data is referenced to fuselage body axes according to right-handed sign conventions.

a	Horizontal distance from pivot axis to spring line of action, feet
a_n	Normal acceleration, g
a_x	Longitudinal acceleration, g
b	Reference span, feet
CG	Center of gravity, fraction of chord
C_L	Lift coefficient
C_m	Pitching moment coefficient
c	Reference chord, feet
c	Viscous retarding moment
d	Perpendicular distance from the CG to the oscillation axis, feet
F_a	Load applied to tail tiedown, lbf
f	Frequency of oscillation, cycles per second
g	Acceleration of gravity, ft/sec^2
h	Altitude, feet
h	Vertical, component of the perpendicular distance from the CG to the oscillation axis, feet
I_o	Moment of inertia about the axis of rotation, $slug\text{-}ft^2$
I_x	Moment of inertia about roll axis, $slug\text{-}ft^2$
I_y	Moment of inertia about pitch axis, $slug\text{-}ft^2$

I_z	Moment of inertia about yaw axis, slug-ft^2
k	Spring constant, lbf/ft
Kα	Flow amplification factor for angle of attack, 1.1
MAC	Mean aerodynamic chord
MSL	Mean sea level
p	Roll rate, de/sec
q	Pitch rate, deg/sec
$\overline{q}$	Dynamic pressure, lbf/ft^2
r	Yaw rate, deg/sec
S	Reference area, ft^2
T_c	Thrust coefficient
u	Control vector
V	Velocity, ft/sec
W	Weight, lbf
W_s	Aircraft and supporting system weight, lbf
x	State vector
x	Amplitude of oscillation
x_a	Horizontal distance from W_s to F_a, feet
X_α, X_{a_n}	Distance of alpha vain and a_n accelerometer forward of CG, feet
z	Measured observation vector
$\overline{Z}$	Vertical CG position from support pivot axis, feet
Z_a	Vertical distance from the support pivot axis to the aircraft reference line, feet
α	Angle of attack, deg
β	Angle of sideslip, deg
δ	Logarithmic decrement

δ_e	Elevator deflection, deg
θ	Pitch angle, deg
ξ	Damping ratio
ϕ	Roll attitude, deg
ω_n, ω_d	Natural and damped frequencies of oscillation, rad/sec

Subscripts

m	Measured
n	Number of cycles
q	Rotary derivative, per rad
α	Static derivative, per deg
δ_e	Control derivative
0	Bias
T_e	Test equipment

INTRODUCTION

Reliable estimates of stability and control derivatives are needed in the design of new aircraft to expand the flight envelope by flight testing and for research of control systems and aircraft handling qualities. Confidence in the values of the derivatives is enhanced when there is agreement between values obtained from flight tests and wind tunnel tests.

In order to obtain reliable and accurate values of the stability and control derivatives, the Dryden Flight Research Center (DFRC) of NASA has developed a technique for extracting the derivatives from flight data. This technique is implemented by a set of Fortran computer programs (reference 1) that is based on a modified maximum likelihood estimator that uses the Newton-Raphson algorithm to perform the required minimization of the derivatives.

DFRC has an ongoing flight test program in which the derivatives are extracted from flight data of selected aircraft. As a part of the program, a PA-30, a light twin-engine general aviation aircraft, has been flight tested and the stability and control derivatives obtained using the DFRC method. The derivatives were compared with those obtained from wind tunnel tests of PA-30 aircraft in the NASA Langley full scale tunnel. The comparison revealed significant differences of derivatives determined by the two methods (see figures 5 through 7). The differences were primarily in the values of the

longitudinal stability derivatives. Since specific and detailed documentation of the instrumentation used in the flight tests was not recorded, it was difficult, if not impossible, to cite a reason for the differences in the values of the derivatives. To resolve the discrepancies it was necessary to repeat the flight tests.

The second flight tests were conducted as a joint venture between the DFRC and California Polytechnic State University as a part of the Graduate Student Program. For these tests, particular attention was given to the calibration and documentation of the instrumentation used. Also, a spring oscillation method (reference 2) was used to determine more accurate values of the moments of inertia. The same aircraft was used for both the Langley wind tunnel (reference 3) and flight tests. The test conditions were primarily the same. When conditions varied, corrections were made in order to make the comparisons valid.

The purpose of this report is to present the results of the new flight test program. Data was obtained with the aircraft in zero, half, and full flap configurations in level unaccelerated flight with the landing gear retracted. The flight tests also included flight with the conditions of zero flaps and zero thrust. The data was analyzed using the modified maximum likelihood technique to extract the longitudinal stability and control derivatives. The derivatives were plotted as functions of angle of attack using various graphical arrangements to show variations of wind tunnel and flight determined values at zero flap settings. Also, data was displayed to show the effects of flap deflection and thrust variation on the longitudinal stability derivatives.

DESCRIPTION OF AIRCRAFT AND INSTRUMENTATION

The aircraft tested was a light twin-engine low-wing monoplane with retractable landing gear. A three view drawing of the PA-30 is shown in figure 1, and the reference axes is shown in figure 2. The geometric and mass parameters of the aircraft are listed in Tables 1 and 2. The wing airfoil section is a NACA 64_2 A215 airfoil. The wing has five degrees of dihedral with zero twist and is placed at two degrees of incidence with respect to the fuselage reference line. The horizontal tail is an all-moveable type, with an overall deflection range from 16 degrees trailing edge up to 5 degrees trailing edge down. The horizontal tail has a trailing edge trim tab that moves in the same direction as the tail. The tab has a deflection ratio (tab deflection to tail deflection) of approximately 1.5.

The only modification to the aircraft was the addition of a hydraulic control system and a remote pilot/control system used in other flight test efforts.

The instrumentation consisted of a standard package used to measure stability and control parameters. This package included three-axis angular rate gyros, attitude gyros, and linear accelerometers in addition to various air data instruments. The locations of the instruments requiring positional correction before the data is used in the computer analysis are listed in Table 3.

The angle of attack and angle of sideslip data were measured using vanes mounted on an instrumentation boom located approximately 3.3 and 3.64 feet, respectively, forward of the right wing tip.

The dynamic pressure ($\bar{q}$), velocity, and altitude were calculated, using a Fortran computer program, from the static and dynamic pressures sampled by the pitot static system onboard the aircraft. The pitot tube probe was located approximately 14 feet from the aircraft centerline under the left wing. The two static ports were located on the sides of the rear fuselage. A radar altimeter, with a range of from zero to 5000 feet, was also used to check the calculated altitude.

The control deflections of the stabilator, ailerons, and rudder were also recorded along with left throttle position, engine RPM, and manifold pressures. The instrumentation analog information was routed through signal conditioning circuits and a pulse code modulator (PCM), and subsequently transmitted to ground based recording equipment by way of an FM/FM transmitter. All of the instruments were calibrated approximately one week prior to the flight tests.

FLIGHT MANEUVERS

All the data was collected on two flights that yielded a total of 97 longitudinal flight maneuvers. Three maneuvers were neglected because of excessive time dropouts and data spikes in the output. Three more maneuvers were dropped for exceeding tolerable angle of attack bounds. The remaining 91 maneuvers were used for the analysis.

The longitudinal stability and control maneuvers consisted of a set of five standard elevator pulses of approximately seven seconds duration. The magnitude of the elevator impulse was such that it yielded a total change of angle of attack from 3 to 6 degrees. These maneuvers were followed by two series of a "3-2-1-1"-multistep elevator

pulse of approximately 11 seconds duration. Both the standard elevator pulse and the "3-2-1-1"-multistep elevator pulse are illustrated in figure 3, which includes an example of an in-flight elevator input (δ_e) of each type.

The "3-2-1-1"-multistep elevator pulse technique is a maneuver that fulfills certain frequency requirements needed in the parameter identification technique used. Theoretically this impulse contains frequencies both above and below the aircraft's natural frequency of the short-period mode (see reference 4).

The maneuvers were performed with the four flight conditions or aircraft configurations most often used within the aircraft's flight envelope. These configurations included settings of zero flaps, half flap (15°), and full flaps (27°) at a nominative thrust coefficient, and a setting of zero flaps with a thrust coefficient of zero. A set of maneuvers was also performed at approximately 300 feet over a flat level surface (a dry lake bed) to compare the computed pressure altitude with the altitude measured by the radar altimeter.

The maneuvers were flown in non-turbulent conditions at altitudes from 7500 to 13000 feet MSL. Data was obtained at several angles of attack for each configuration with the aircraft flying straight and level. The angle of attack ranged from .5° to 8° for the zero flap with nominative thrust coefficient flight condition. For the one half and full flap settings with nominative thrust coefficient flight condition, angles of attack ranged from 3.5° to 8.5°. The angles of attack for the flight condition of zero flap setting and zero thrust coefficient were 1.0°, 5.5°, and 10.0°.

All of the flight maneuvers were flown with the landing gear retracted, and without the use of stability augmentation equipment. The flight tests were conducted with a center of gravity position of 16% (±2%) MAC, but was corrected to a reference position of 10% MAC for analysis. The weight ranged from 3600 to 3450 pounds during the two flights, and was known to be within 2% to 3% for each maneuver.

DATA PROCESSING

A number of different methods and techniques were used to manage and maintain the quality of the flight data, and every attempt was made to maintain the integrity of the outputs.

The recorded flight parameters, which are listed in Table 4, were uniformly passed through a 40 hertz passive filter on board the aircraft. The data was sampled by a 10-bit pulse code modulation (PCM) digital system at 200 samples per second. The sampling rate was reduced to 100 samples per second and an analytic computer program was used to filter the buffet noise from the data channels requiring it. The filter used a notch at a frequency of 19.4 hertz and a third order low-pass at 20 hertz. All of the known phase shifts and spikes in the data that were caused by instrumentation or sampling anomalies were corrected or removed. The data was ultimately thinned to 25 samples per second for analysis.

The air data which included the parameters of true velocity, geopotential pressure altitude, corrected dynamic pressure, and corrected static pressure were calculated from the measured static and dynamic pressures.

The moments of inertia (I_x, I_y, I_z) were calculated using the data obtained from the spring oscillation tests of the aircraft. The experimental method is shown in Appendix B. The numerical results are in Table 2.

METHOD OF ANALYSIS

An iterative method of coefficient variance minimization was used to find the longitudinal stability and control derivatives from flight data. This iterative technique, sometimes called the Newton-Raphson algorithm, was incorporated into a general parameter estimation computer program.

The mathematical formulation of this method can be described in probabilistic terms. For each possible estimate of the unknown parameters, a probability can be obtained that the calculated aircraft response time histories will take on those values actually observed. Those estimates are chosen, and the equation's coefficients are adjusted so that the probability is maximized. The describing equation's coefficients are the stability and control derivatives. The best maximization comes when the initial probable values are closest to the actual observed values. This process is referred to as a maximum likelihood formulation of the problem.

The maximum likelihood estimation technique can be made to include a priori information that can come from wind tunnel studies, previous flight tests, and other sources of predicted derivatives. The method that uses a priori information is called the modified maximum likelihood estimator (MMLE) and is explained in detail in reference 1.

In this analysis of the flight test data a priori information was not used.

The full-scale wind tunnel obtained stability derivatives were used as starting values for the computer analysis. A complete description of the digital computer program (MMLE3) used in the extraction of the derivatives is in reference 5. A brief outline of the equations of motion used in MMLE3 is included in Appendix A.

The maximum likelihood estimator also contains an objective measure of the validity of the estimates of the stability and control derivatives. These uncertainty levels are proportional to the Cramer-Rao bounds described in reference 6. These bounds are analogous to the standard deviations of the estimated stability derivatives. The greater the uncertainty level of the coefficient, the greater the uncertainty will be of the estimated derivative. The best uncertainty approximation comes by comparing confidence levels of the same derivatives obtained from different flight maneuvers. Thus by comparing uncertainty levels of derivatives obtained from several maneuvers, the validity of the stability and control derivatives can be checked.

A set of stability and control derivatives as a function of angle of attack are chosen by fairing the derivative values from plotted results at a particular angle. The fairings take into account the derivative grouping and the uncertainty levels which lead to a choice of a single representative derivative value at the corresponding angle of attack. The faired derivative values from the wind tunnel and previous flight tests are listed in Tables 5 and 6, respectively.

RESULTS AND DISCUSSION

The nondimensional stability derivatives C_{m_α}, C_{m_q}, $C_{m_{\delta_e}}$, C_{L_α} and $C_{L_{\delta_e}}$ determined from the flight data, and the full-scale Langley wind tunnel results were plotted as functions of angle of attack (alpha). These results along with representative, faired, values from the previous flight tests are graphically superimposed for easy comparison. The graphs clearly illustrate an improvement in the results.

The uncertainty levels of each derivative are indicated on the graphs as a vertical bar. The magnitude of the vertical bars is multiplied by five to improve viewing.

A typical example of a pulse and "3-2-1-1" longitudinal maneuver time history of angle of attack, pitch rate, pitch attitude, normal acceleration and elevator input is shown in figure 4. The dotted lines in these plots are the maximum likelihood method curve fit to the actual time history. As can be seen, there is little difference between the two curves.

Zero Flap Deflection, Constant Thrust Setting

The thrust settings for these maneuvers were chosen by the pilot to maintain the desired angle of attack.

The negative value of C_{m_α} shown in figure 5a indicates a stable aircraft. The graph also shows that the magnitude of C_{m_α} increases at larger values of angle of attack for the flight test data, but decreases for the wind tunnel data. The results of the second flight test are shown to be nearer to the values of the wind tunnel results than are the results of the first flight test. The C_{L_α} vs alpha curves

shown in figure 5b indicates good agreement between the derivatives obtained from the second flight and wind tunnel tests. The C_{L_α} determined from the first flight test differed as much as 27% lower than the tunnel derivatives. The results of the second flight tests are clearly an improvement.

The longitudinal rotary derivative, C_{m_q}, in figure 5c remained negative, constant, and stable over its angle of attack range. There were no wind tunnel estimates available for comparison for C_{m_q}. However, the second flight test results are shown to be consistently larger in magnitude than the first test results.

The $C_{m_{\delta_e}}$ vs alpha curve shown in figure 5d reveals that both the first and second flights had curves with negative slopes. The values of the derivatives from the second flight are shown to be nearer to the values of the wind tunnel estimates. As shown in figure 5e, the values of $C_{L_{\delta_e}}$ very closely agreed with the wind tunnel estimates for the range of angle of attack tested. Good agreement between the values of $C_{L_{\delta e}}$ determined from wind tunnel and the first flight was obtained only near zero alpha. Excellent agreement for values of $C_{L_{\delta_e}}$ for the entire range of alpha tested is shown for wind tunnel and second flight determined values. In fact, the most significant improvement of second flight results over first flight results is obtained in the values of $C_{L_{\delta e}}$.

The trimmed elevator position, $\delta_{e_{trim}}$, corrected to the reference CG position of 10% MAC, is plotted as a function of angle of attack in figure 5f. The pitching moment coefficient, C_{m_o}, and lift coefficient, C_{L_o}, biases are plotted as a function of angle of attack in figures 5g and 5h, respectively. These biases are calculated values

in the pitching moment and lift coefficient equations in the maximum likelihood procedure.

Flap Deflection Effects

Figures 6a through 6h show the effects of flap deflection on the stability derivatives. The derivative values from the second flight test for half and full flaps are graphically superimposed with the zero flap derivative curve. The half and full flap derivative curves from the first flight were also graphically superimposed for easy comparison. There were no wind tunnel values available for the half and full flap conditions.

The second flight showed more variation between the half and full flap derivative values of C_{m_α} and C_{L_α} than did the first flight. As can be seen in the C_{m_α} and C_{L_α} curves, figures 6a and 6b, the half flap derivative values did not change significantly from the no flap values. On the other hand, the C_{m_α} for the full flap condition were greater than those for the full range of alpha, and magnitudes of C_{L_α} for the full flap condition were lower.

Both the C_{m_q} and $C_{m_{\delta_e}}$ derivatives become more negative in magnitude at lower angles of attack as flap deflection increases from zero to half, but does not change as the deflection increases from half to full position. See figures 6c and 6d.

Figure 6e reveals that flap position does not significantly affect $C_{L_{\delta_e}}$ values at low alpha. However, there are appreciable differences in the values of $C_{L_{\delta_e}}$ determined from first and second flight tests.

Figure 6f shows the effect of flap deflection on $\delta_{e_{trim}}$, which shows a decrease of $\delta_{e_{trim}}$ as flap deflection increases. The values of

C_{m_o} and C_{L_o} are also plotted, figures 6g and 6h, to show flap deflection effects.

Thrust Effects

The effects on the longitudinal stability and control derivatives caused by varying thrust are depicted in figures 7a through 7h. Each graph shows the derivatives obtained for the second flight at T_c of approximately zero, along with the first flight and wind tunnel curves at zero T_c. The nominative thrust coefficient from the second flight is thought to be the same as the wind tunnel value of 0.1. Both the second flight nominative and wind tunnel thrust coefficient curves are graphically superimposed to show the change in derivatives.

Figure 7a shows that the values of C_{m_α} obtained from both flight tests are less negative than the wind tunnel values for zero T_c. There is no significant difference in the C_{m_α} values for nominative and zero T_c conditions. Therefore, the conclusion is that thrust variation does not significantly affect the value of C_{m_α} for the range of T_c tested. Figure 7b reveals that C_{L_α} for zero T_c obtained from the second flight test are closer to the zero T_c wind tunnel values for small angles of attack than are values from the first flight test. The opposite is the case for higher angles of attack. For the second flight test the nominative T_c derivatives are larger than the zero T_c values. This is also true for the wind tunnel nominative and zero T_c values. The conclusion supported by this data is that increase of thrust causes an increase of C_{L_α}.

As seen in figure 7c, C_{m_q} values determined from the second flight test are less negative for the condition of zero T_c than for

nominative T_c. Values of C_{m_q} determined from the first flight test are even less negative. Again, there are no wind tunnel estimates for C_{m_q}.

As shown in figure 7d, for both the wind tunnel and second flight tests, values of $C_{m_{\delta_e}}$ for the nominative T_c condition are lower than for the zero T_c condition. First flight tests values of $C_{m_{\delta_e}}$ for the zero T_c condition are larger than either the wind tunnel or second flight test values. The conclusion drawn from this data is that an increase of thrust decreases the values of $C_{m_{\delta_e}}$.

There is very little difference in the derivative $C_{L_{\delta_e}}$, shown in figure 7e, as T_c changes. This is also the case for the wind tunnel estimates. The conclusion is that thrust variation has little effect on $C_{L_{\delta_e}}$.

The trimmed elevator deflection is shown for the zero T_c condition in figure 7f. The moment coefficient and lift coefficient biases are shown in figures 7g and 7h. Both biases did not change appreciably as the thrust coefficient changed.

CONCLUDING REMARKS

A complete set of longitudinal stability and control derivatives were obtained from 91 maneuvers. The conditions of flight that were analyzed included zero, half, and full flap configurations with a nominal thrust coefficient, and with no flaps and zero thrust coefficient. The flight time histories of all the maneuvers had good matches with the modified maximum likelihood estimator (MMLE3) predictions, which subsequently led to good derivative estimates. Knowing the aircraft's vertical and longitudinal center of gravity, to within 4$ and 2% respectively, was a major factor in obtaining good matching

of the time histories. The second flight estimates agreed with wind tunnel estimates much better than those of the first flight. The exact cause for the differences between the first and second flight results is not known.

Specifically, the conclusions drawn from this study are:

1. The C_{m_α}, C_{L_α}, $C_{m_{\delta_e}}$, and $C_{L_{\delta_e}}$ estimates at the zero flap condition had closer agreement with the wind tunnel estimates than did the first flight estimates. The most significant improvement of the second flight results over the first was in $C_{L_{\delta_e}}$.

2. An increase of flaps from zero to half position shows little effect on C_{m_α} and C_{L_α}, but causes C_{m_q} and $C_{m_{\delta_e}}$ to decrease at lower angles of attack.

3. An increase of flaps above half position causes C_{m_α} to increase and C_{L_α} to decrease.

4. Thrust variation has little effect on C_{m_α}, $C_{L_{\delta_e}}$, C_{m_o}, and C_{L_o} for the range of T_c tested.

5. An increase of thrust causes an increase in C_{L_α}, but a decrease in C_{m_q} and $C_{m_{\delta_e}}$.

TABLE 1

GEOMETRIC CHARACTERISTICS OF THE PA-30 AIRPLANE

WING:	
Area, including aileron and flaps, ft^2	178
Span, ft	35.98
Mean aerodynamic chord, ft	5
Dihedral, leading edge, deg.	5
Incidence, deg.	2
Length of flap, each, ft	9.2
Length of aileron, each, ft	6.3
Total aileron area, ft^2	14.1
Total flap area, ft^2	20.2
STABILATOR:	
Total area, ft^2	32.5
Span, overall, ft	12.5
Mean aerodynamic chord, ft	2.7
VERTICAL TAIL:	
Fin area, ft^2	9
Rudder area, ft^2	5.2
Rudder mean aerodynamic chord, ft	1.2

TABLE 2

AIRCRAFT MASS CHARACTERISTICS

Full Fuel Condition, Without Pilot and Co-pilot	
Weight, lb	3355.
CG, percent of reference chord	15.9
I_x, slug • ft^2	2601.
I_y, slug • ft^2	2052.
I_z, slug • ft^2	4713.
Empty Fuel Condition, Without Pilot and Co-pilot	
Weight, lb	2992.
CG, percent of reference chord	15.7
I_x, slug • ft^2	2526.
I_y, slug • ft^2	2038.
I_z, slug • ft^2	4608.

TABLE 3

INSTRUMENT LOCATIONS RELATIVE TO
REFERENCE CENTER OF GRAVITY

Instrument	Distance forward of reference CG, ft	Distance right of aircraft centerline, ft	Distance below reference CG, ft
α	3.48	17.06	.833
β	3.83	17.625	1.4
a_n	-.158	.885	.862
a_x	-.158	.885	.862
a_y	-.158	.885	.862

TABLE 4

RECORDED PARAMETERS

Parameter	Resolution
Angle of attack, deg	.03
Angle of sideslip, deg	.05
Airspeed, ft/sec	.15
Altitude, ft	.2
Pitch rate, deg/sec	.12
Roll rate, deg/sec	.12
Yaw rate, deg/sec	.08
Pitch attitude, deg	.34
Roll attitude, deg	.39
Yaw attitude, deg	.34
Normal acceleration, g	.01
Longitudinal acceleration, g	.002
Lateral acceleration, g	.001
Aileron position, total, deg	.04
Rudder position, deg	.06
Stabilator position, deg	.03
Throttle position, left, units	.009
Engine manifold pressure, right and left, PSIA	.04
Engine RPM, right and left	.09

TABLE 5

FULL SCALE WIND TUNNEL DERIVATIVE ESTIMATES

a) Zero Flap, Gear Up, $T_c = 0.1$

Derivative per degree	α (degrees) -2	0	2	4	6	8	10	12
C_{m_α}	-.0125	-.0135	-.016	-.0170	-.0175	-.0180	-.0190	-.0195
C_{L_α}	.093	.093	.092	.091	.090	.087	.082	.064
C_{m_q}			not available					
$C_{m_{\delta e}}$	-.051	-.053	-.054	-.053	-.051	-.049	-.047	-.045
$C_{L_{\delta e}}$	.018	.019	.020	.020	.018	.016	.013	.011

b) Zero Flap, Gear Up, $T_c = 0$

Derivative per degree	α (degrees) -2	0	2	4	6	8	10	12
C_{m_α}	-.0170	-.0170	-.0170	-.0170	-.0170	-.0170	-.0170	-.0170
C_{L_α}	.088	.088	.087	.085	.083	.080	.077	.048
C_{m_q}			not available					
$C_{m_{\delta e}}$	-.046	-.046	-.046	-.046	-.046	-.045	-.042	-.039
$C_{L_{\delta e}}$	.016	.016	.015	.014	.012	.009	.006	.003

TABLE 6

FIRST DRYDEN FLIGHT DERIVED DERIVATIVE ESTIMATES

a) Zero Flap, Gear Up, $T_c = 0.1$

Derivative per degree	α (degrees) -2	0	2	4	6	8	10	12
C_{m_α}	--	-.0095	-.0085	-.0080	-.0080	-.0075	-.0070	--
C_{L_α}	--	.0670	.0670	.0680	.0695	.0715	.0770	--
C_{m_q} (per rad.)	--	-14.1	-14.0	-14.0	-13.8	-13.4	-12.8	--
$C_{m_{\delta e}}$	--	.0360	-.0380	-.0395	-.0410	-.0440	-.0440	--
$C_{L_{\delta e}}$	--	.016	.008	.002	.001	0.00	0.00	--

b) Half Flap, Gear Up, $T_c = 0.1$

Derivative per degree	α (degrees) -2	0	2	4	6	8	10	12
C_{m_α}	--	-.0080	-.0080	-.0080	-.0080	--	--	--
C_{L_α}	--	.0750	.0750	.0770	.0775	--	--	--
C_{m_q} (per rad.)	--	-14.7	-15.8	-15.7	-15.4	--	--	--
$C_{m_{\delta e}}$	--	.037	-.042	-.043	-.043	--	--	--
$C_{L_{\delta e}}$	--	.007	-.001	-.005	-.004	--	--	--

TABLE 6 (continued)

c) Full Flap, Gear Up, T_c = 0.1

(degrees)

Derivative per degree	-2	0	2	4	6	8	10	12
C_{m_α}	--	--	-.0065	-.0075	-.0080	--	--	--
C_{L_α}	--	--	.0750	.0770	.0775	--	--	--
C_{m_q} (per rad.)	--	--	-15.8	-15.7	-15.4	--	--	--
$C_{m_{\delta e}}$	--	--	-.042	-.043	-.043	--	--	--
$C_{L_{\delta e}}$	--	--	-.001	-.005	-.004	--	--	--

d) Zero Flap, Gear Up, T_c = 0

(degrees)

Derivative per degree	-2	0	2	4	6	8	10	12
C_{m_α}	--	--	-.0085	-.0080	-.0080	-.0075	-.0070	--
C_{L_α}	--	--	.0760	.0760	.0765	.0770	.0770	--
C_{m_q} (per rad.)	--	--	-14.0	-14.0	-13.8	-13.4	-12.8	--
$C_{m_{\delta e}}$	--	--	-.0370	-.0370	-.0360	-.0340	-.0315	--
$C_{L_{\delta e}}$	--	--	.008	.002	.001	0.0	0.0	--

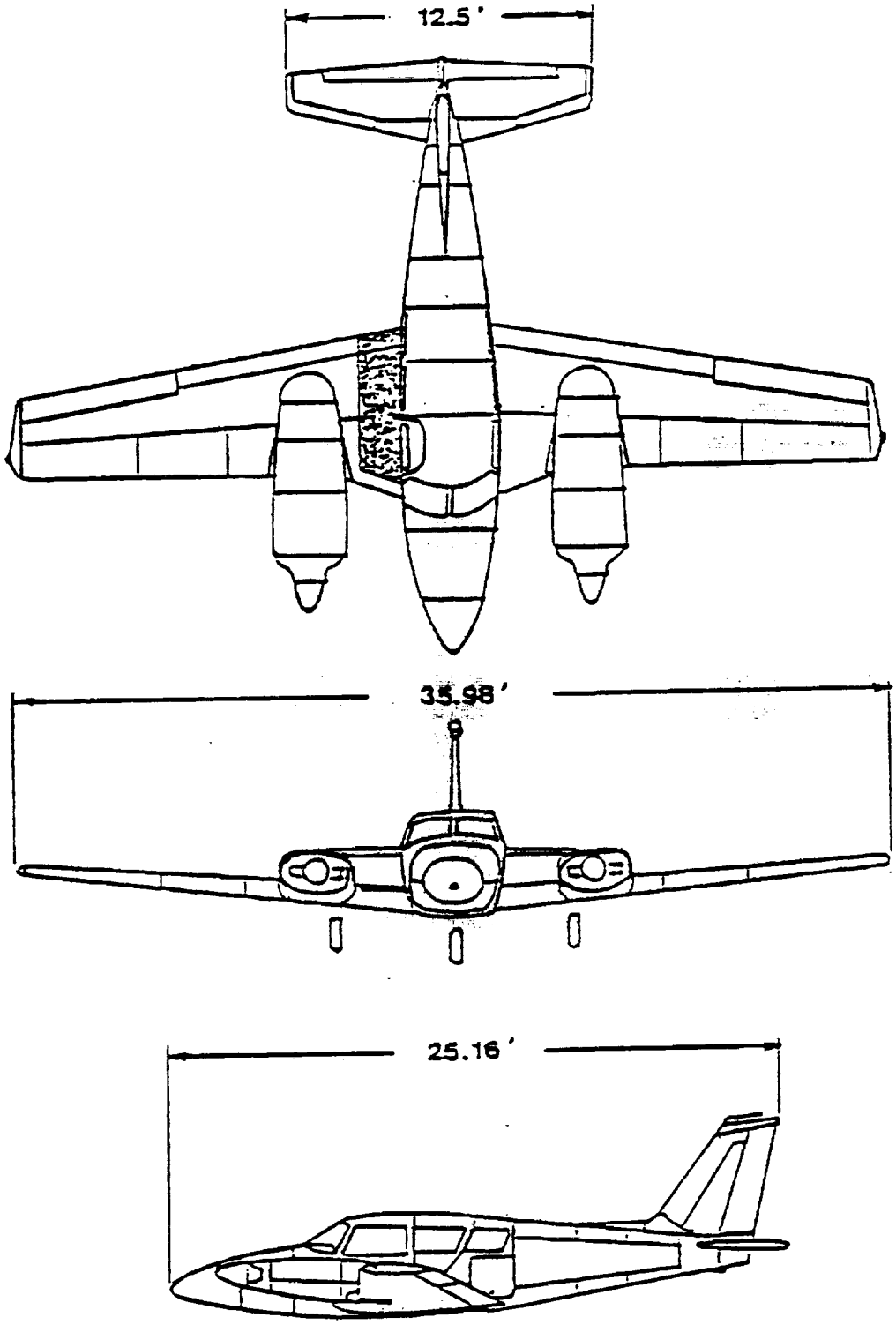

Figure 1. Three view drawing of the PA-30.

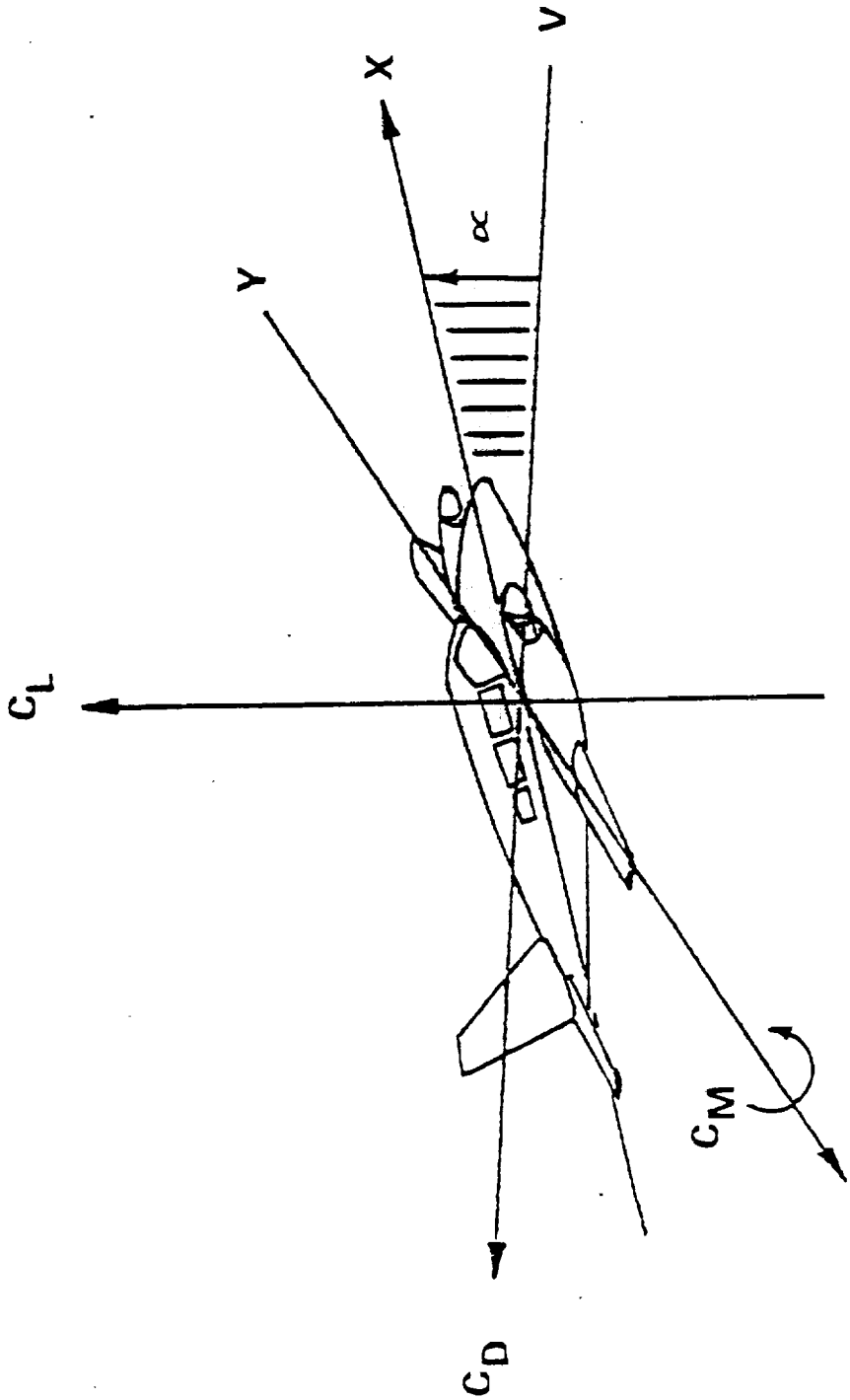

Figure 2. Axis system and positive sense of angles, forces, and moments.

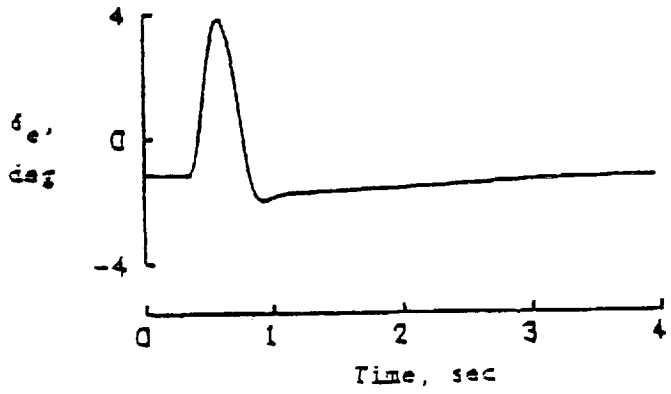

(a) Standard elevator pulse

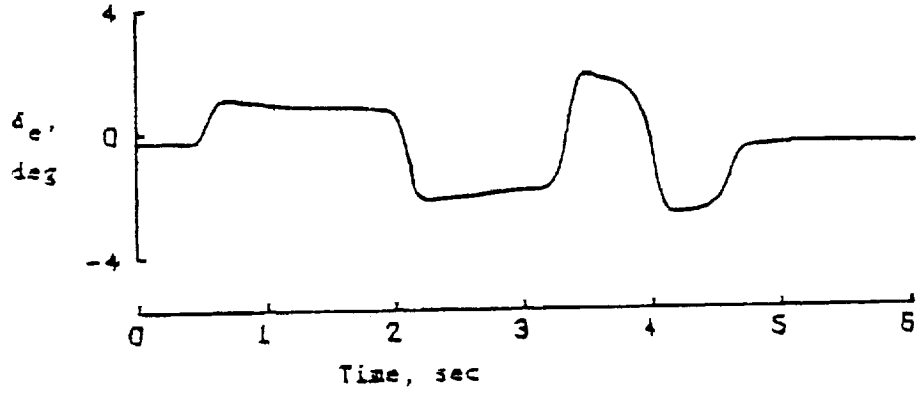

(b) 3-2-1-1 multistep elevator pulse

Figure 3. Longitudinal elevator pulse inputs used.

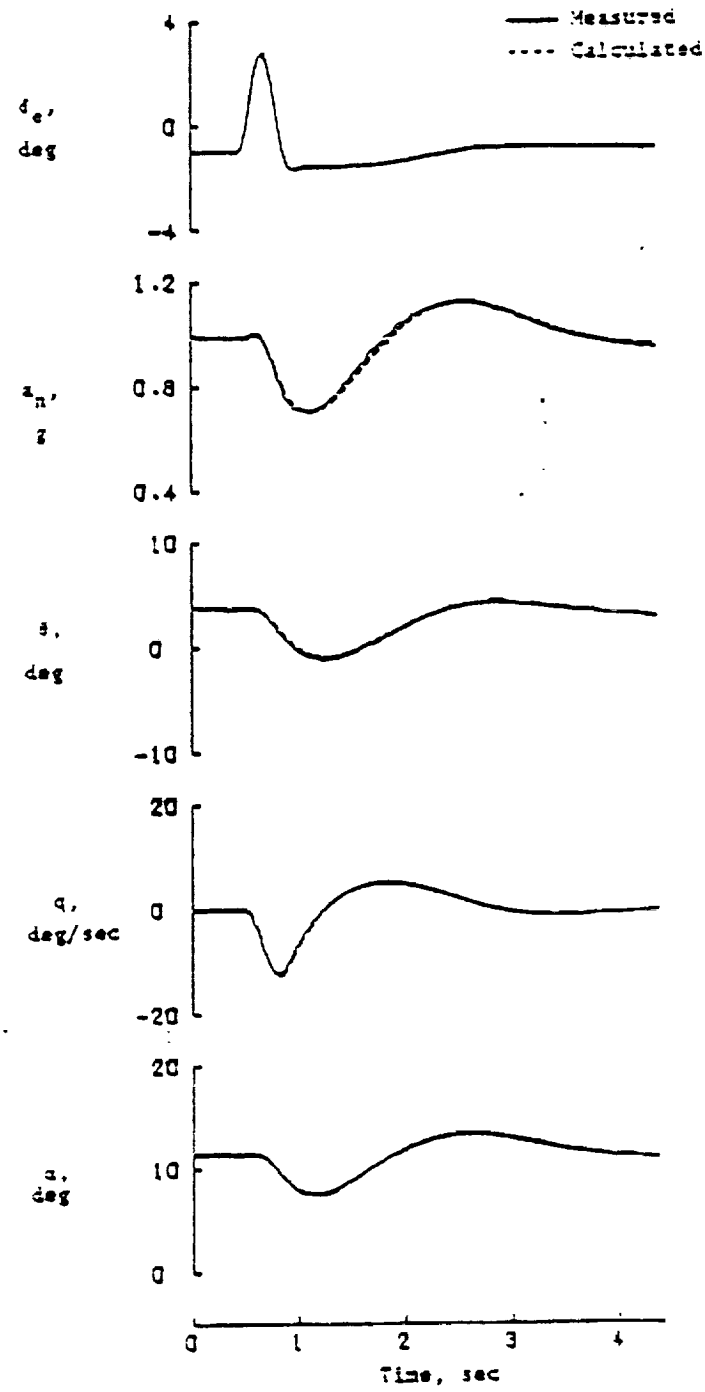

(a) Elevator pulse maneuver

Figure 4. Typical maneuver time histories.

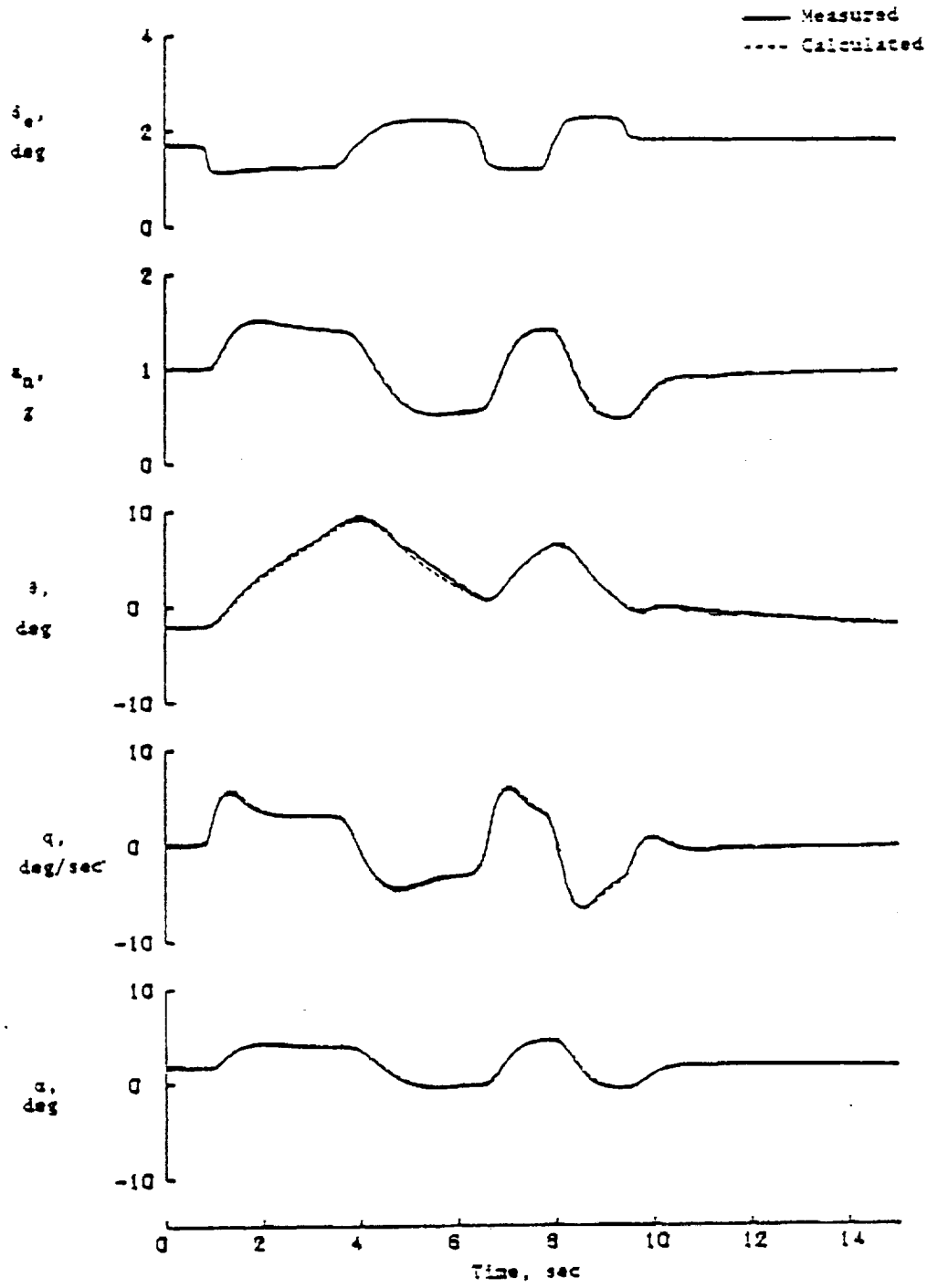

(b) 3-2-1-1 maneuver

Figure 4. Concluded.

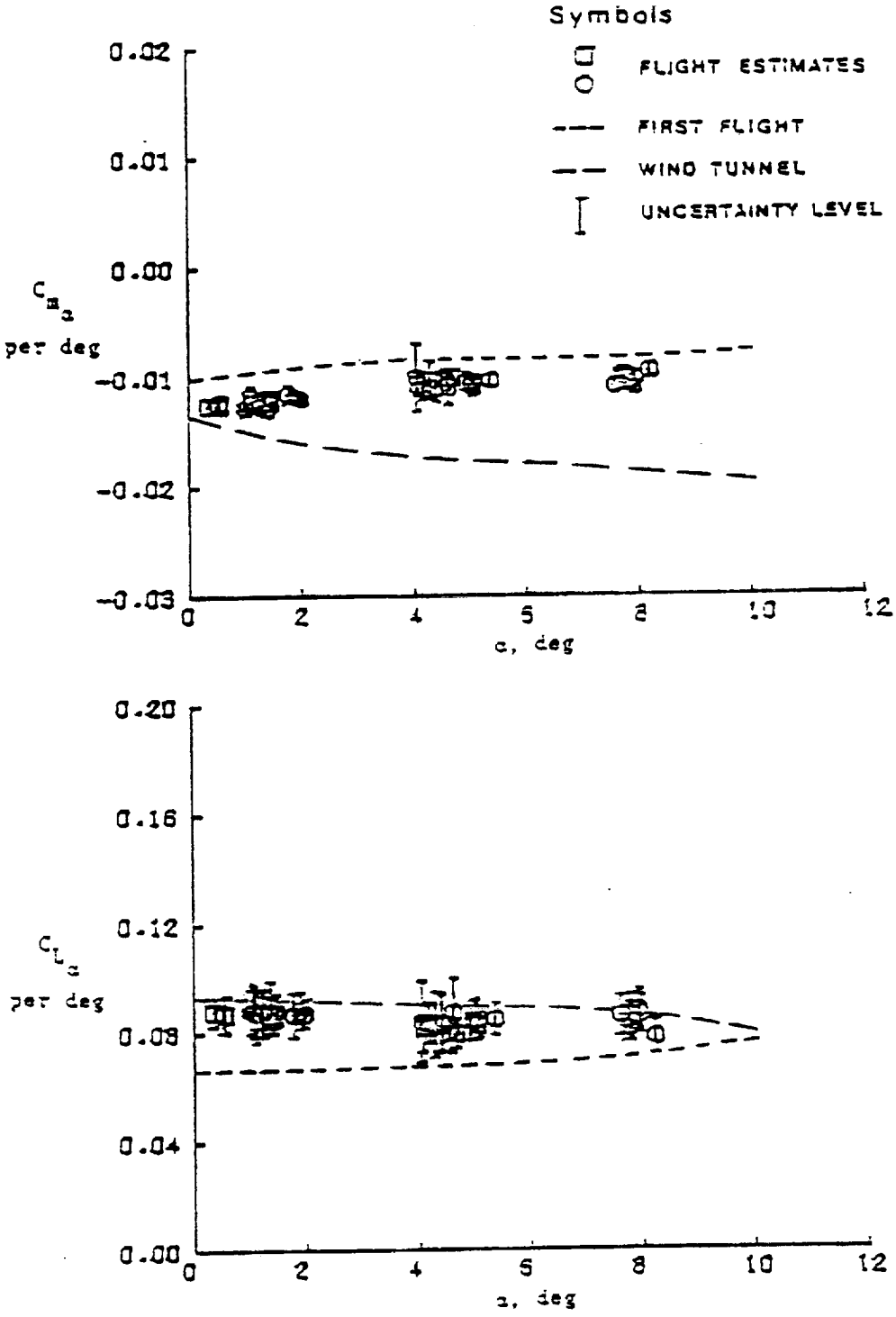

(a) C_{m_α}, (b) C_{L_α}

Figure 5. Stability derivatives at zero flap deflection, and constant nominative thrust setting.

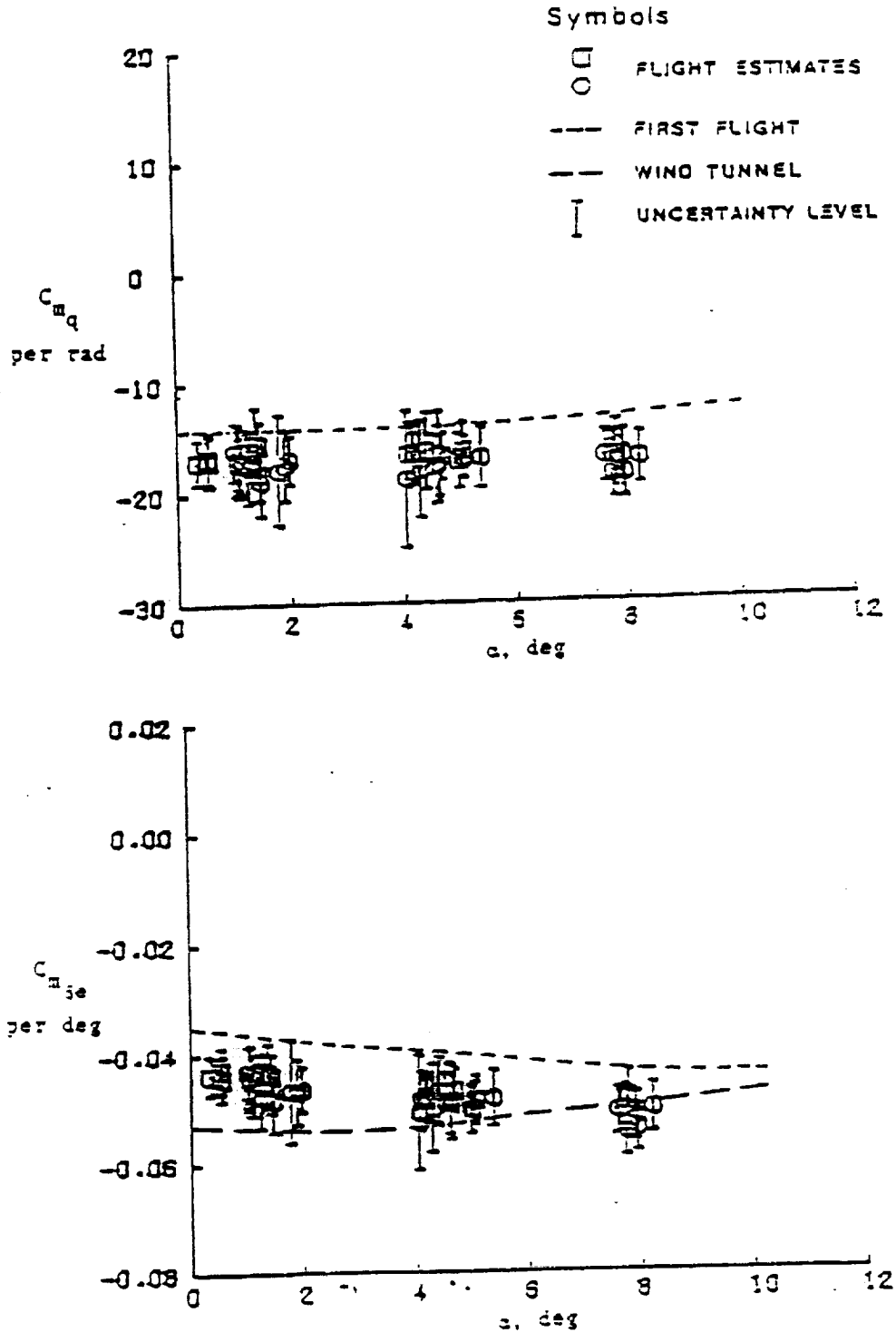

(c) C_{m_q}, (d) $C_{m_{\delta e}}$

Figure 5. Continued.

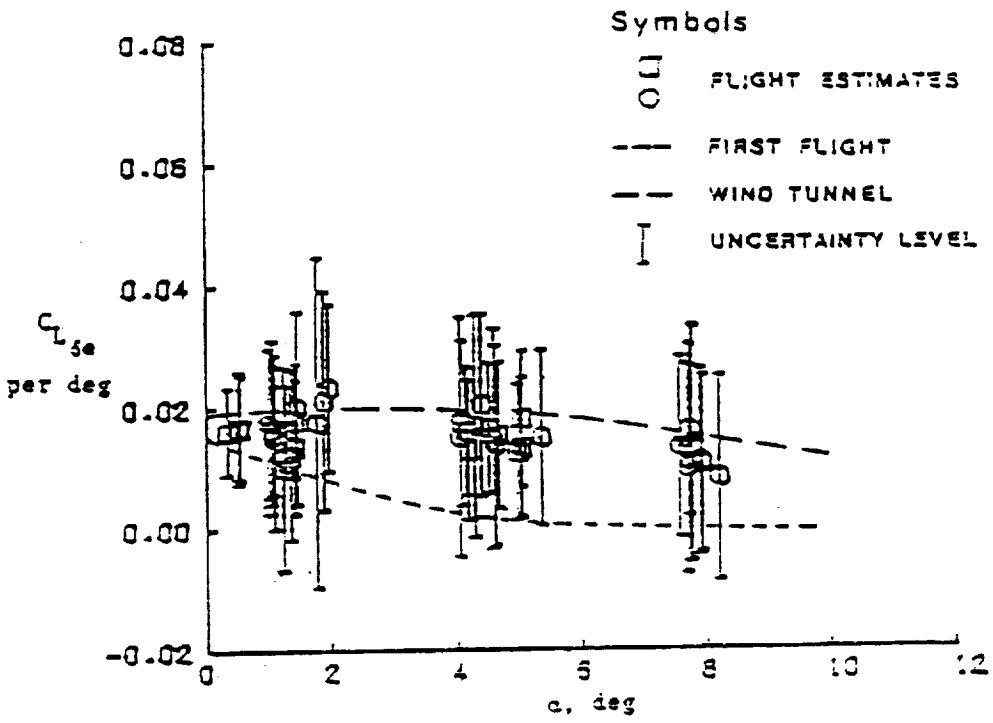

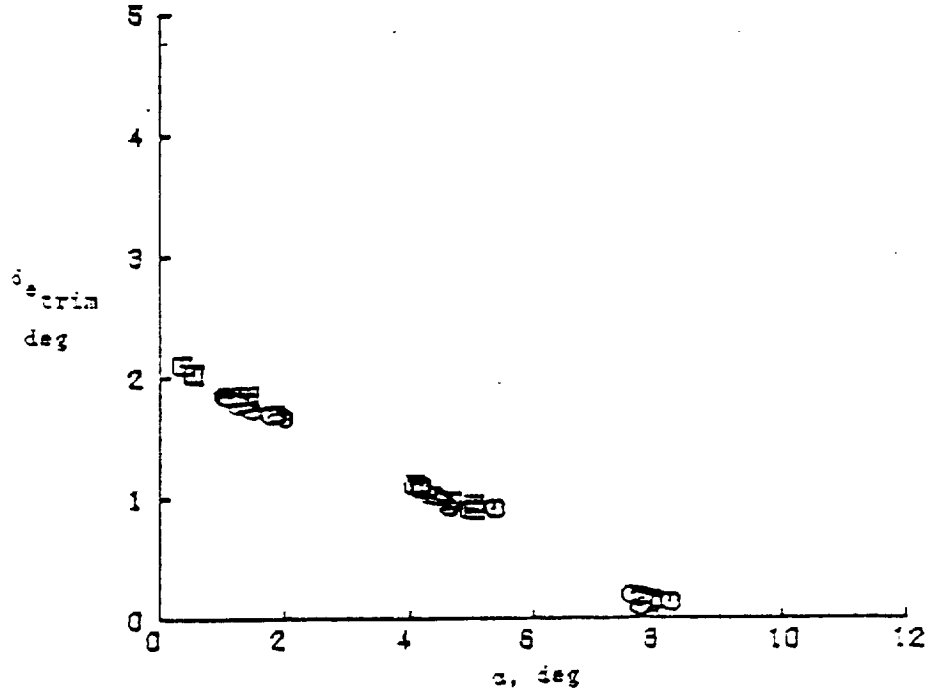

(e) $C_{L_{\delta e}}$, (f) $\delta_{e_{trim}}$

Figure 5. Continued.

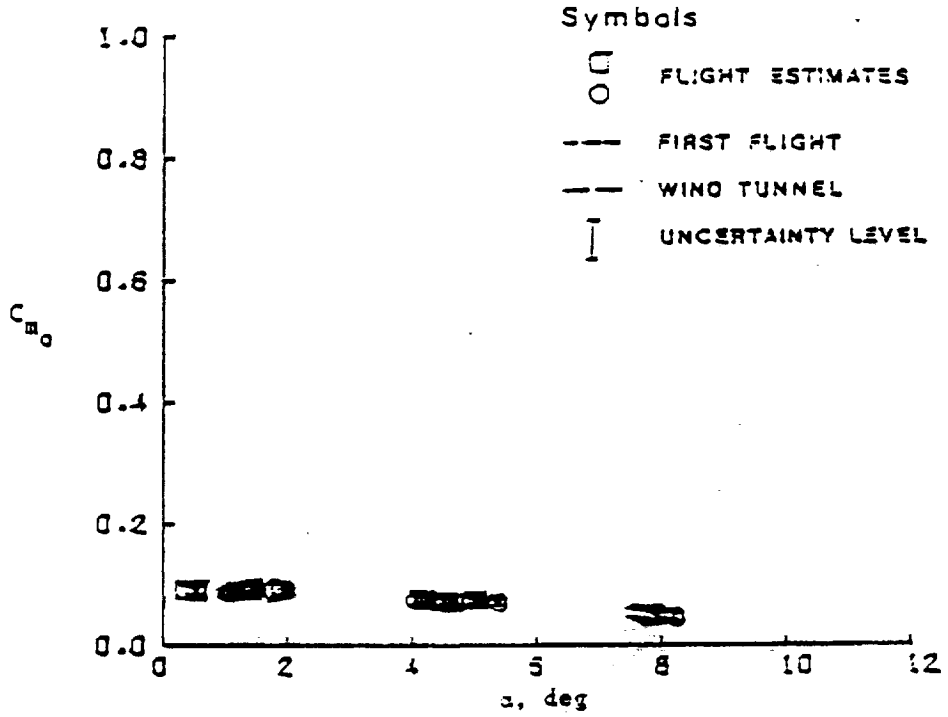

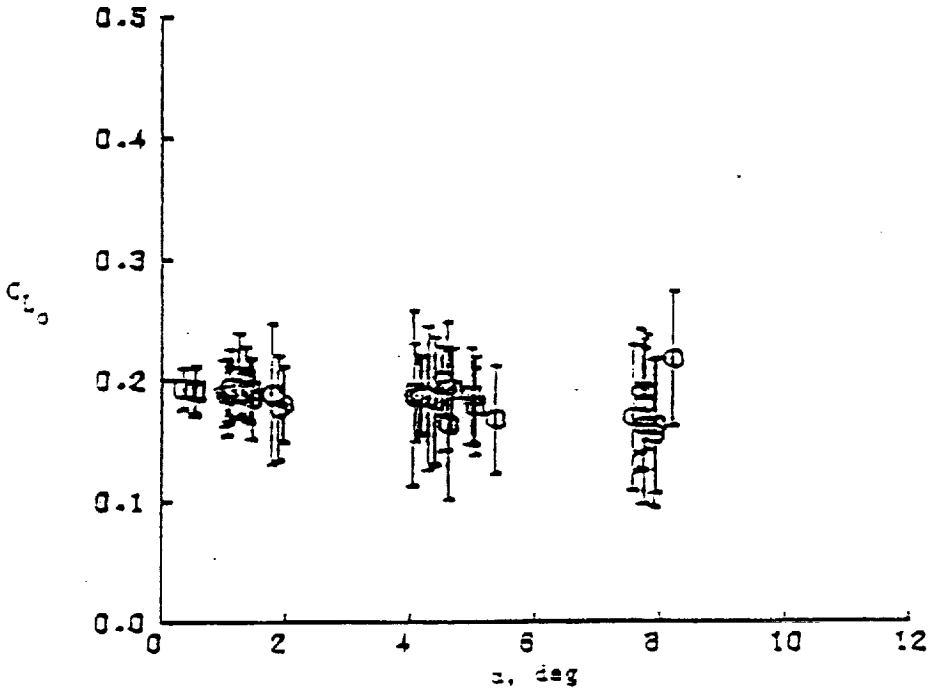

(g) C_{m_o}, (h) C_{L_o}

Figure 5. Concluded.

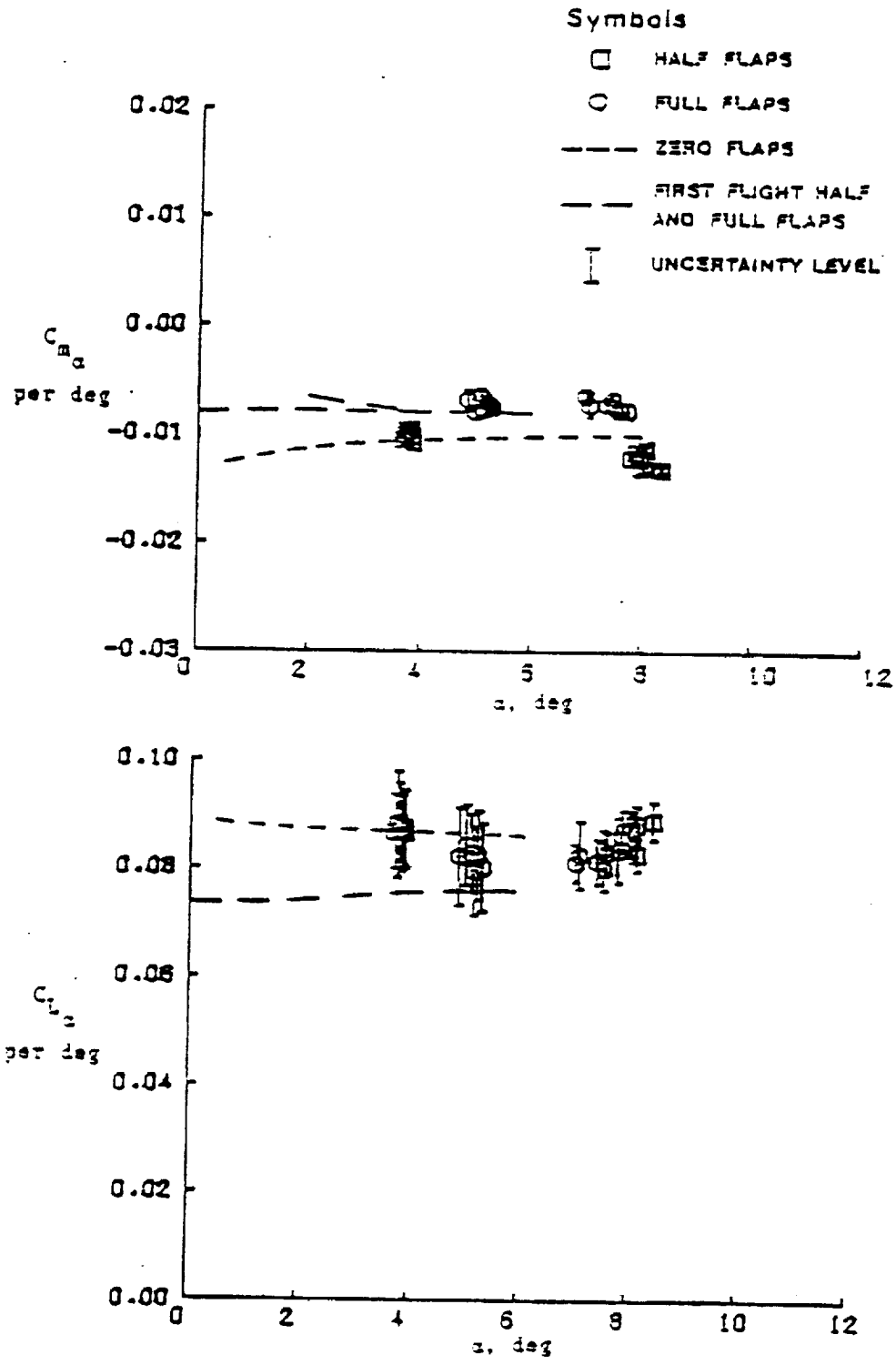

(a) C_{m_α}, (b) C_{L_α}

Figure 6. Effect of flap deflection on stability derivatives.

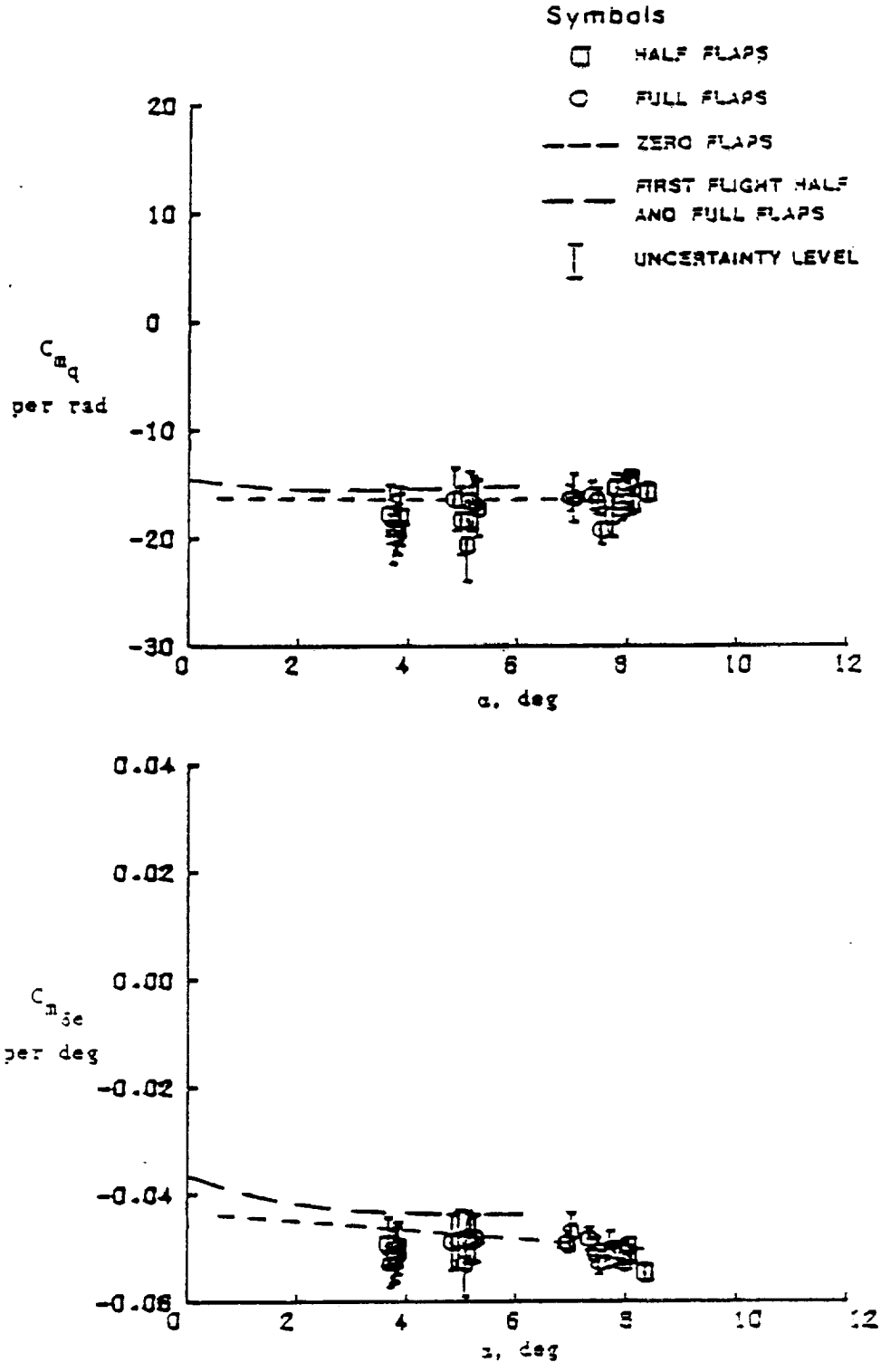

(c) C_{m_q}, (d) $C_{m_{\delta e}}$

Figure 5. Continued.

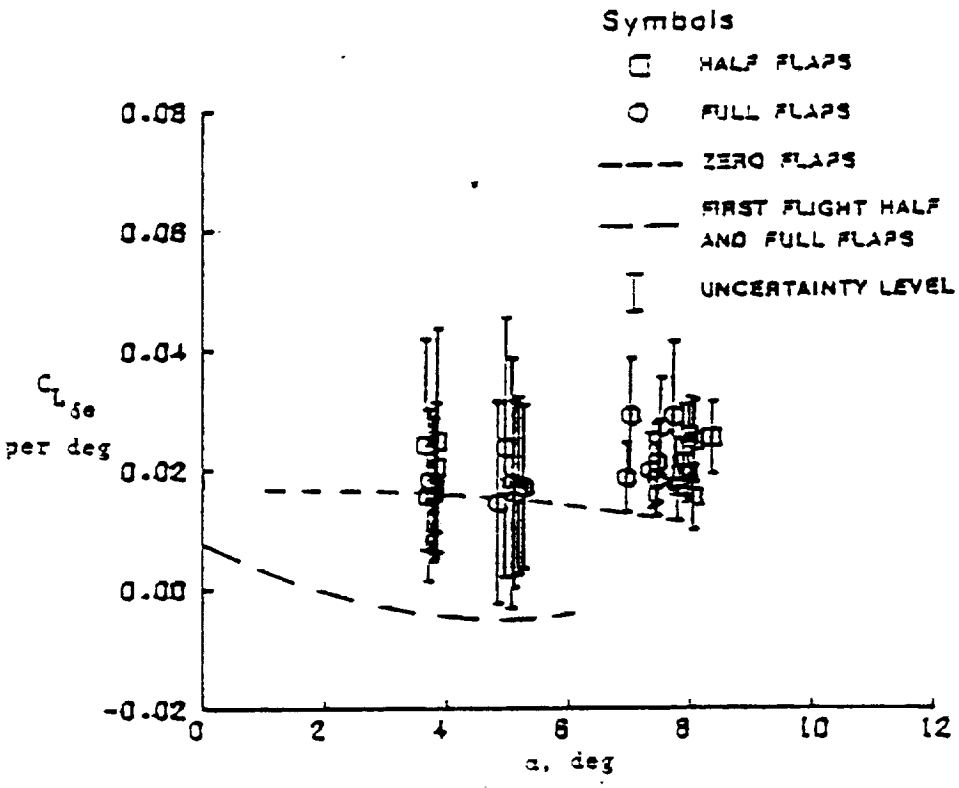

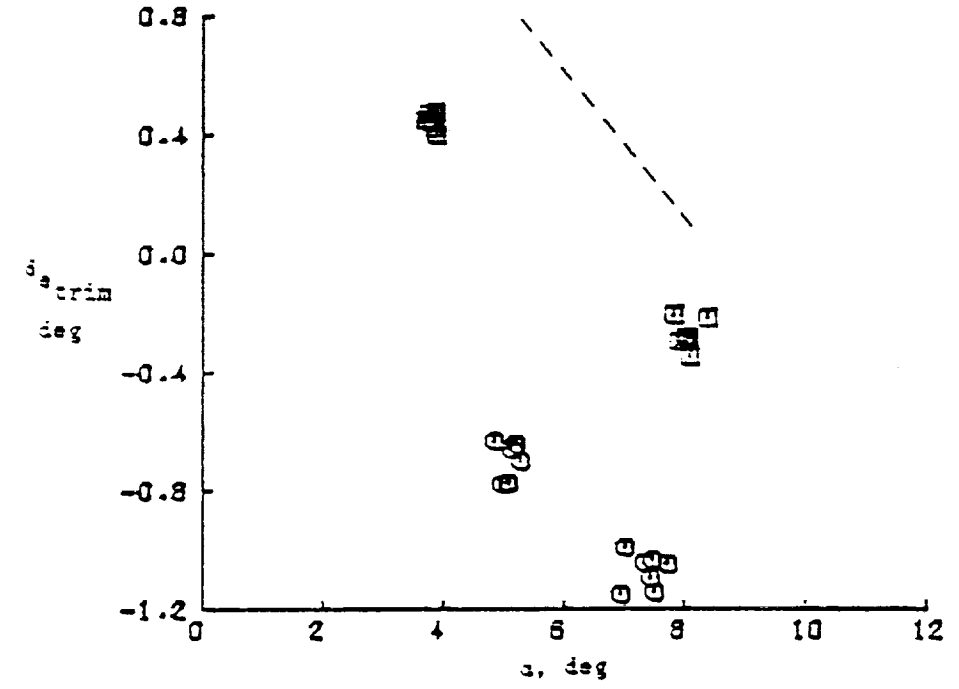

(e) $C_{L_{\delta e}}$, (f) $\delta_{e_{trim}}$

Figure 5. Continued.

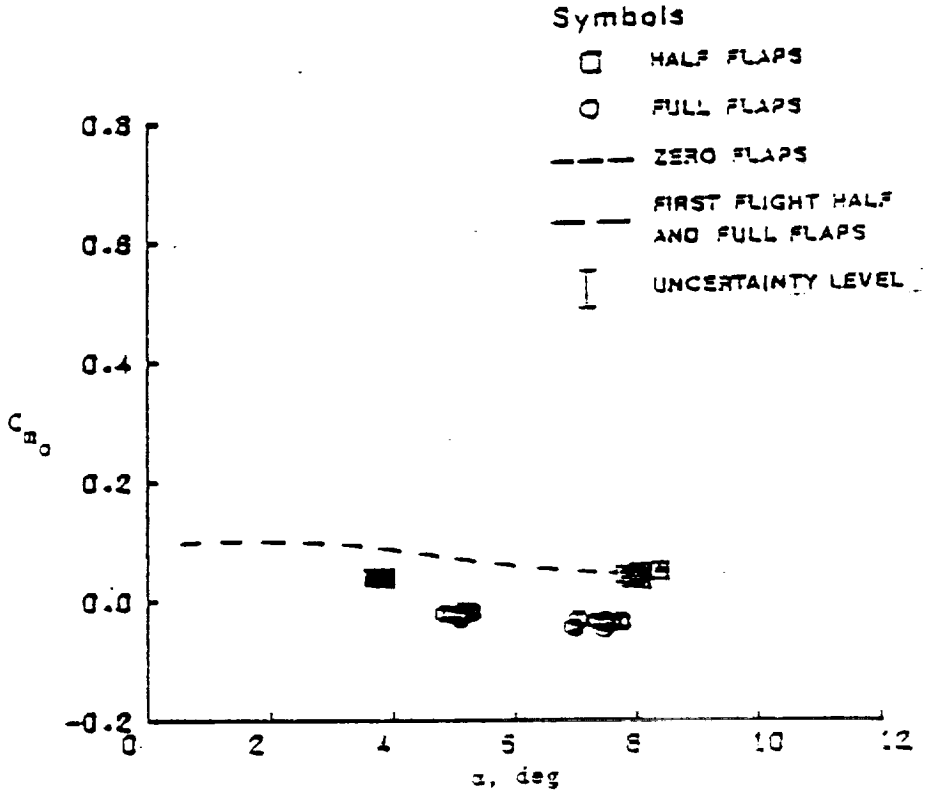

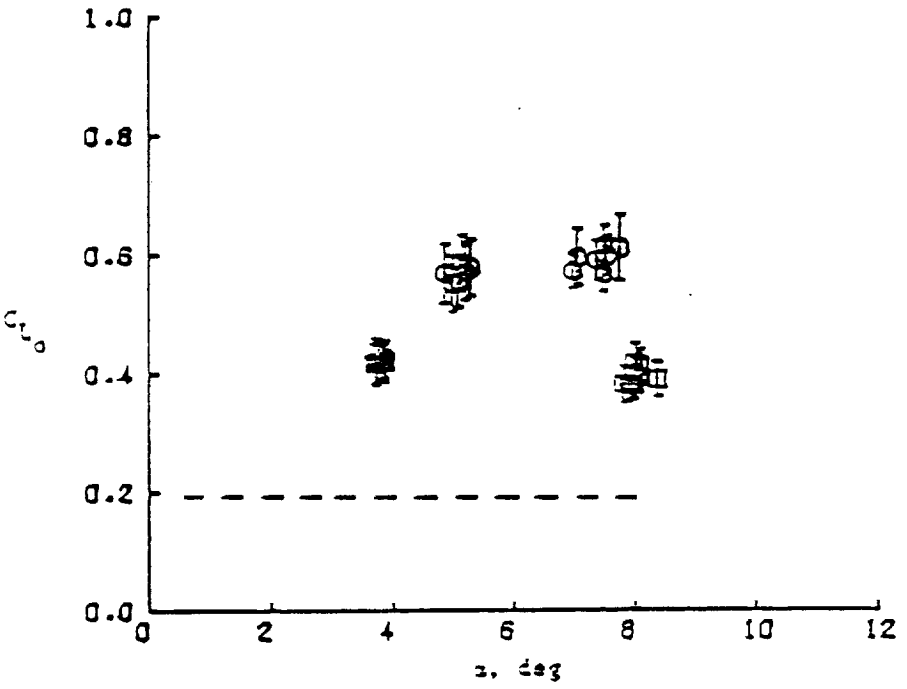

(g) C_{m_0}, (h) C_{L_0}

Figure 6. Concluded.

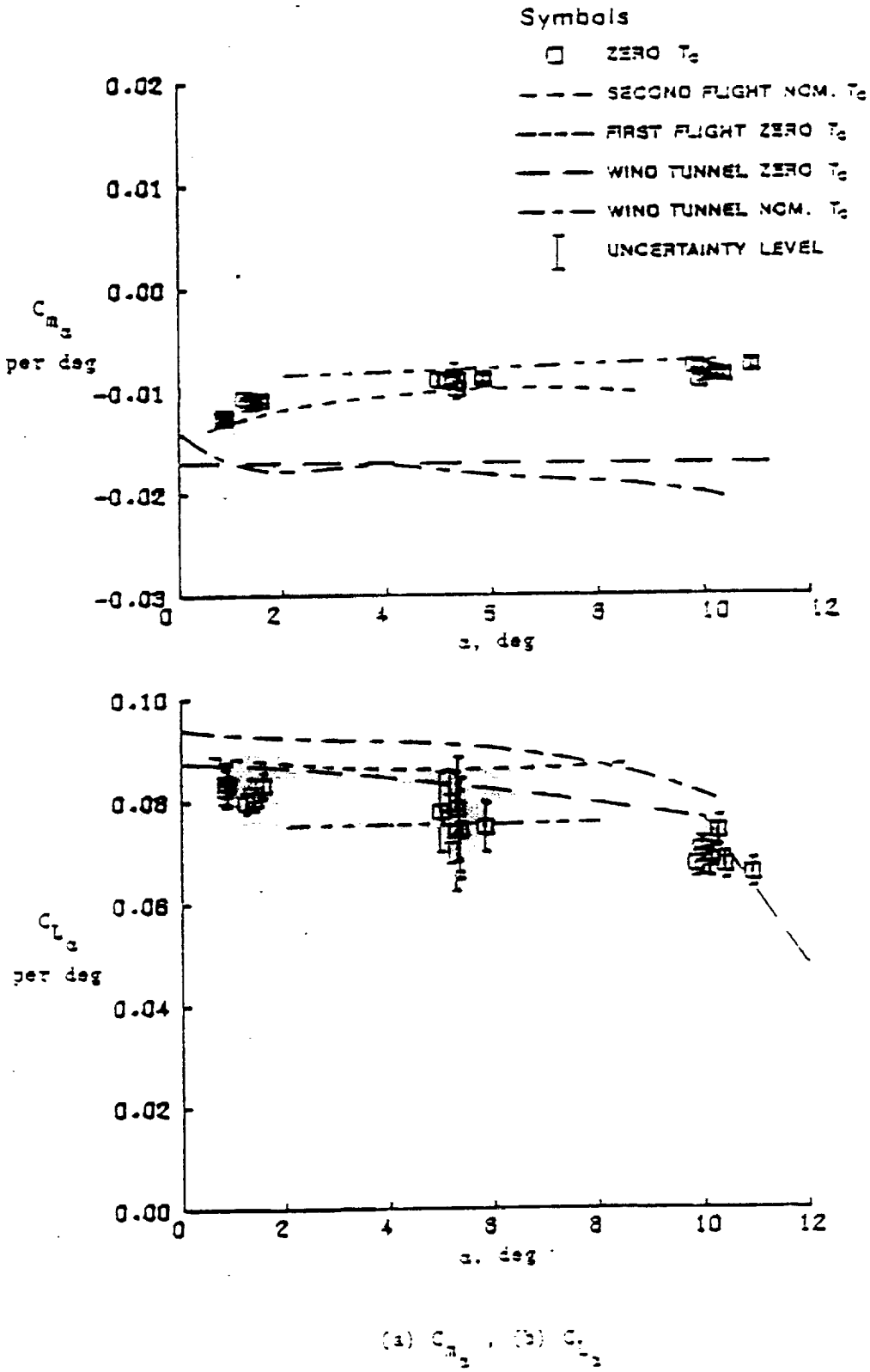

(a) C_{m_α}, (b) C_{L_α}

Figure 7. Effect of thrust on stability derivatives.

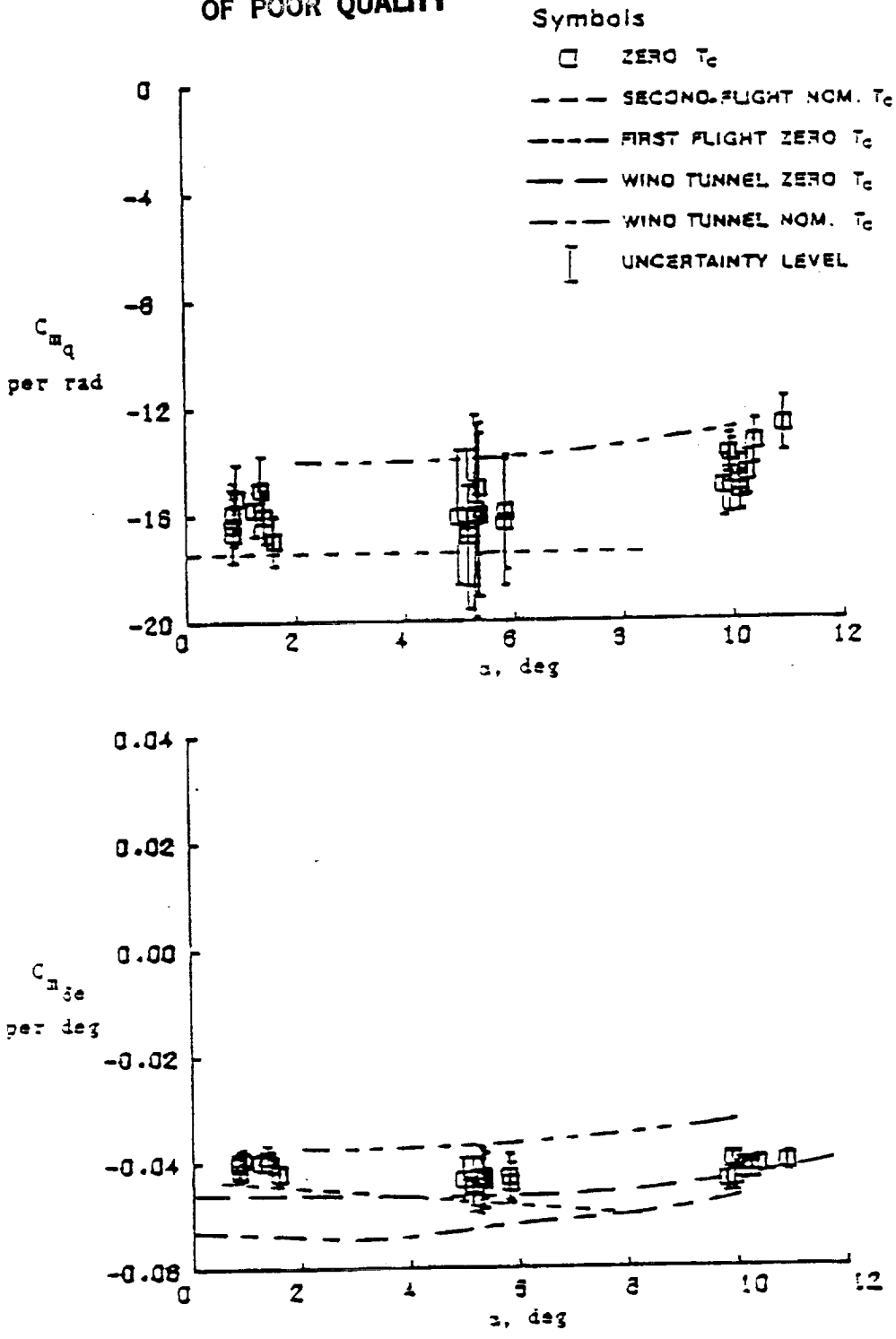

(c) C_{m_q}, (d) $C_{m_{\delta e}}$

Figure 7. Continued.

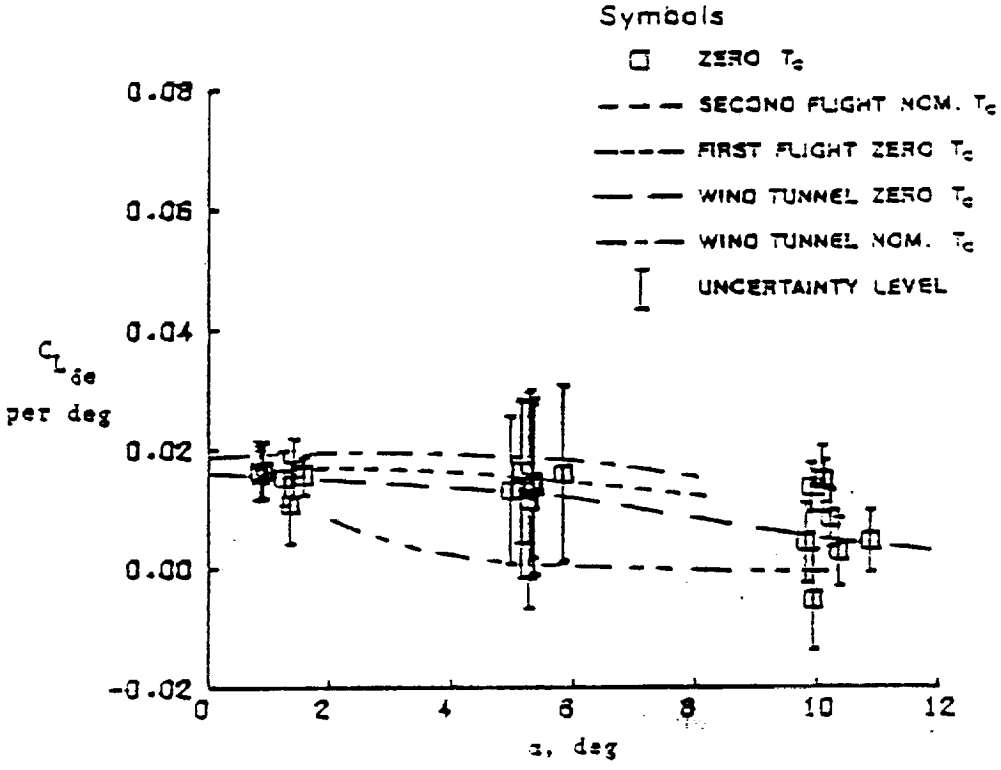

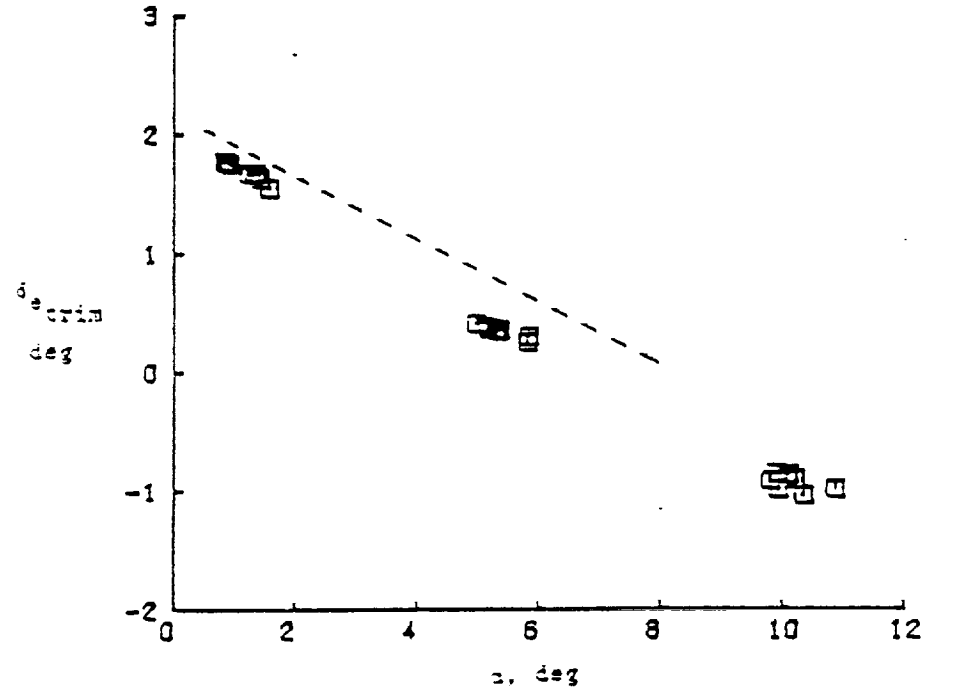

(e) $C_{L_{de}}$, (f) $\delta_{e_{trim}}$

Figure 7. Continued.

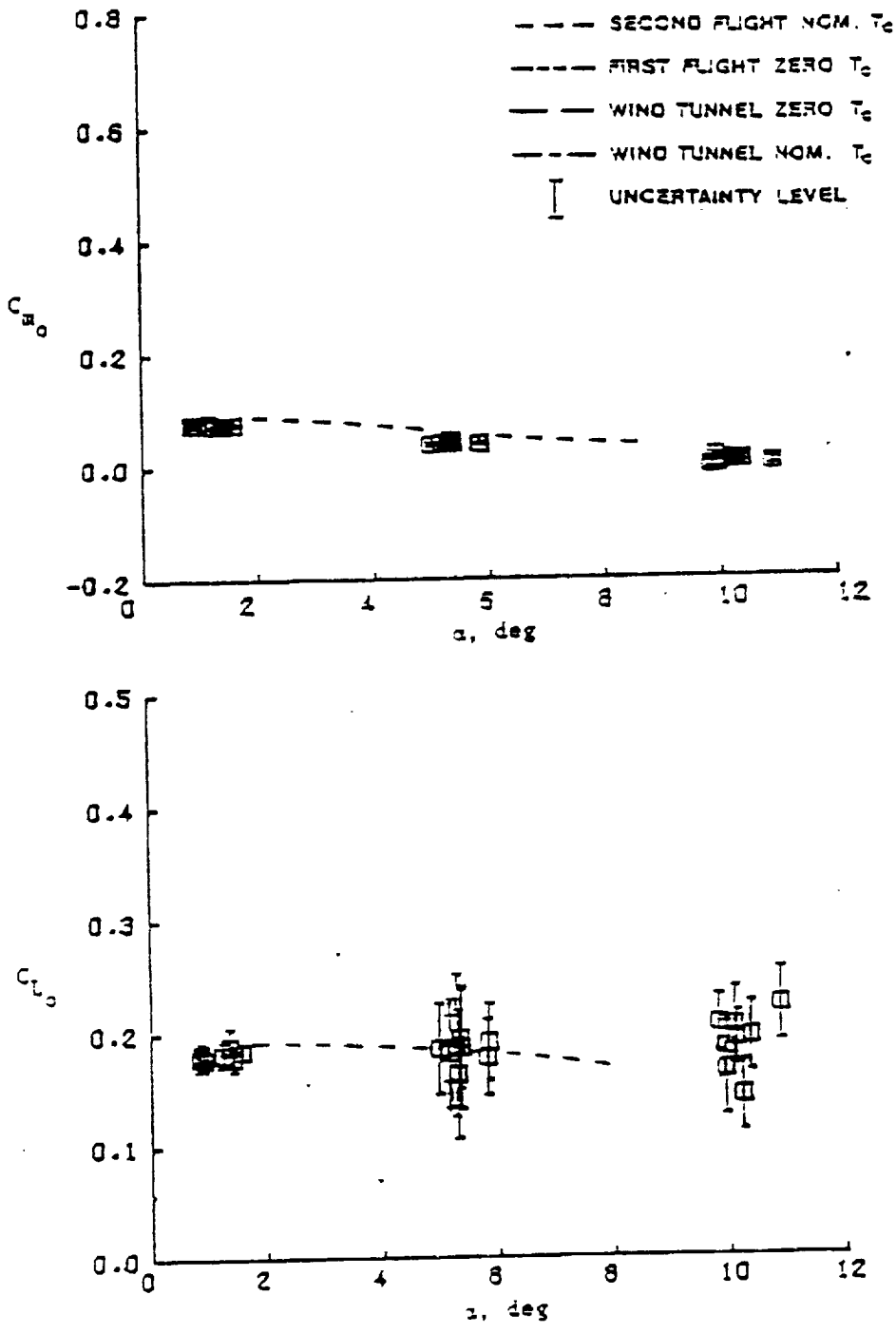

(g) C_{m_0}, (h) C_{L_0}

Figure 7. Concluded.

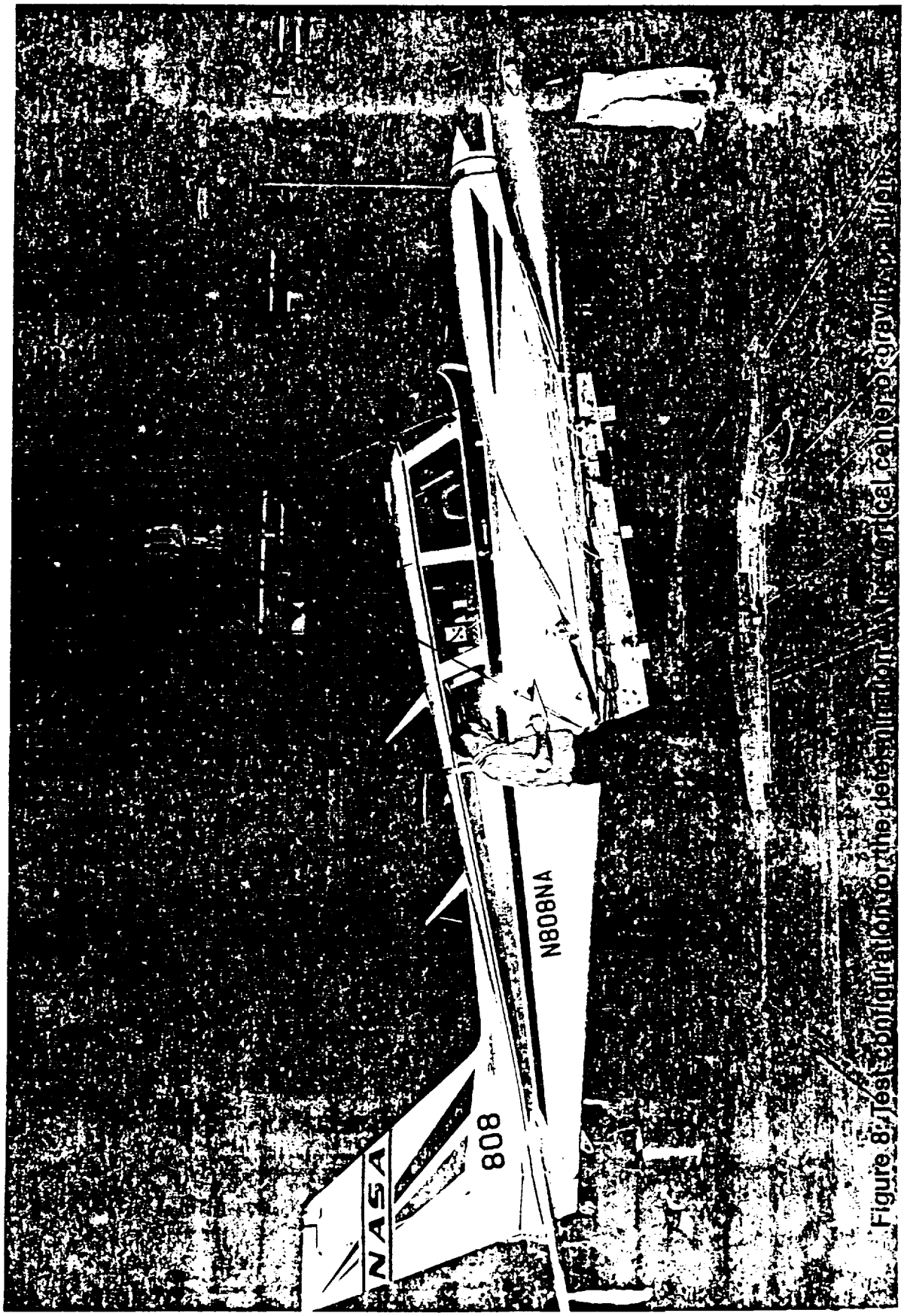

Figure 8. Test configuration for the determination of the vertical center of gravity location.

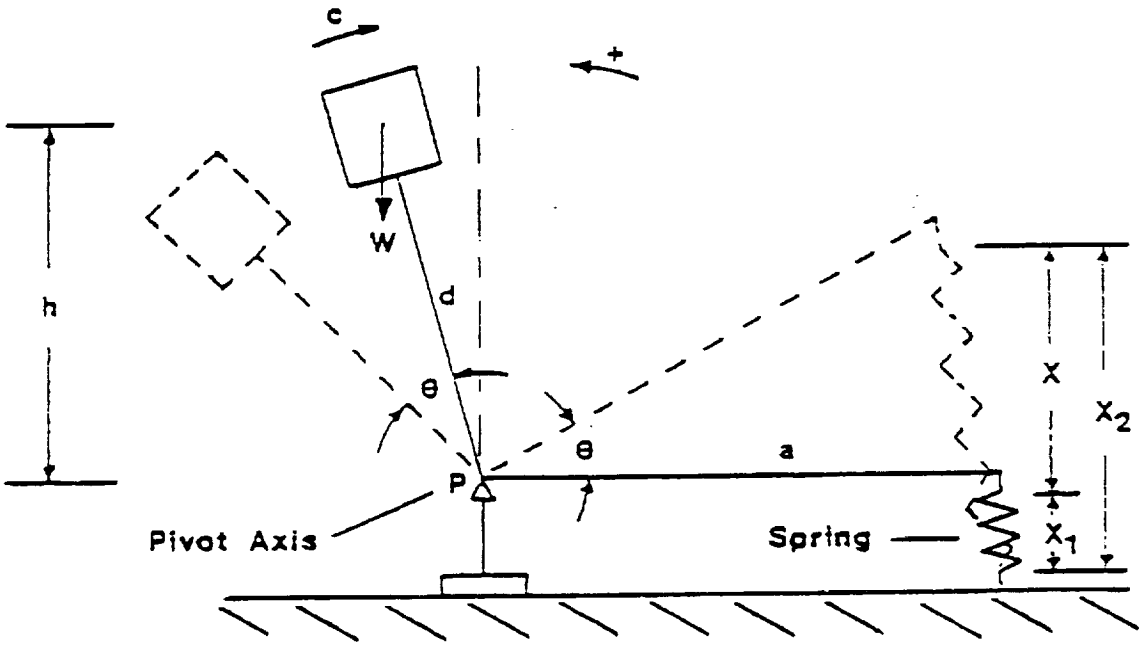

Figure 9. Mass, spring oscillation system.

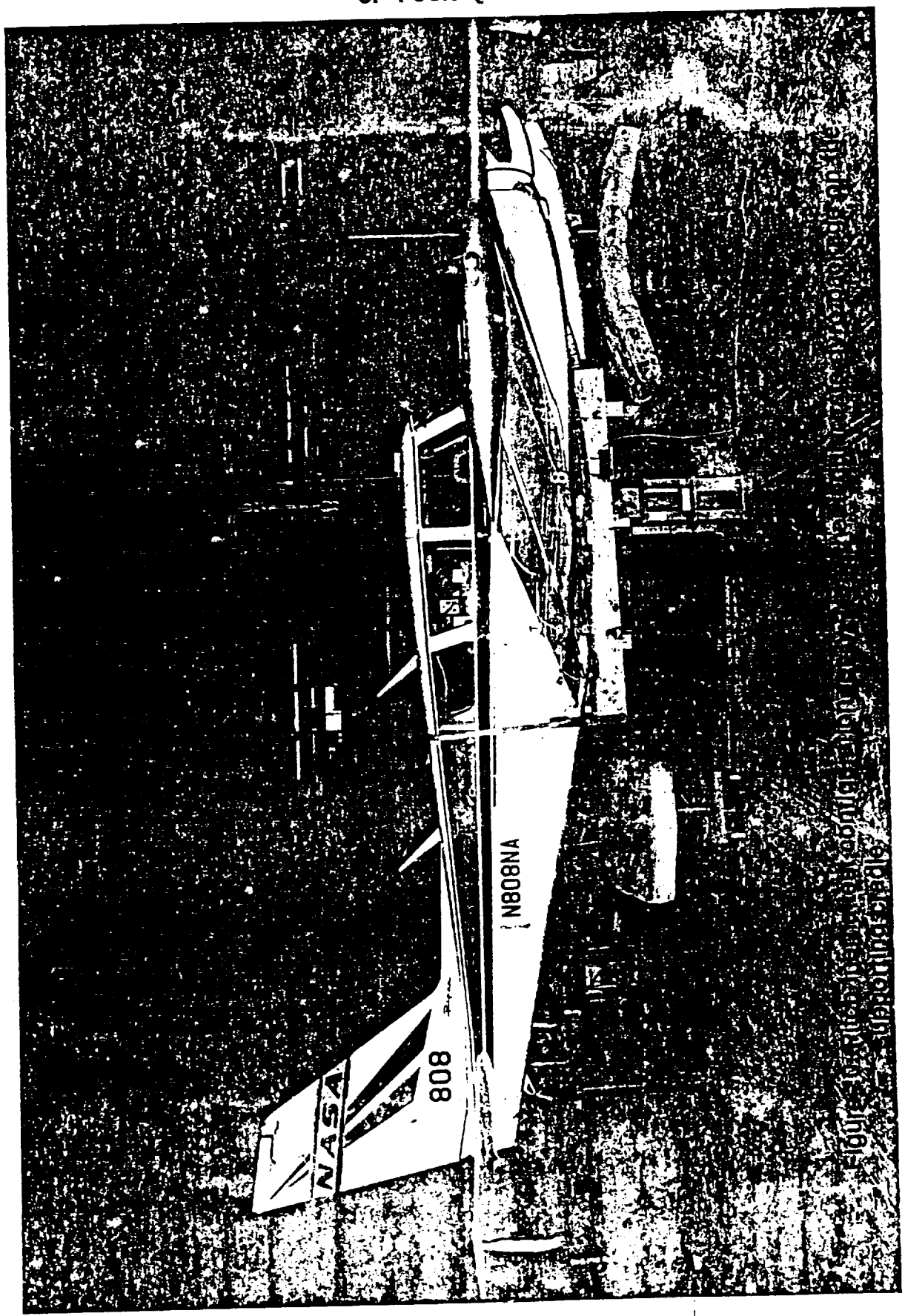

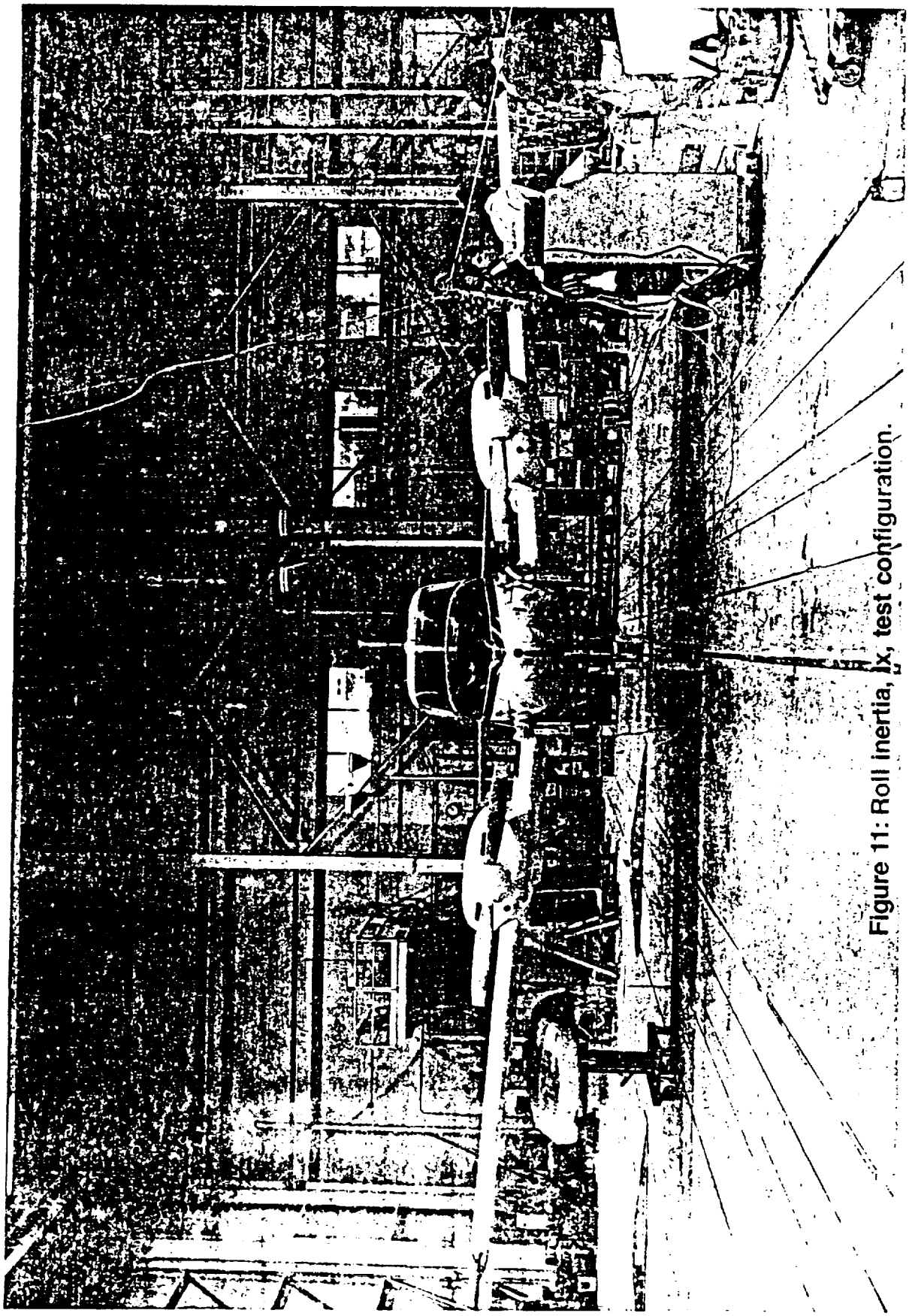

Figure 11: Roll inertia, I_x, test configuration.

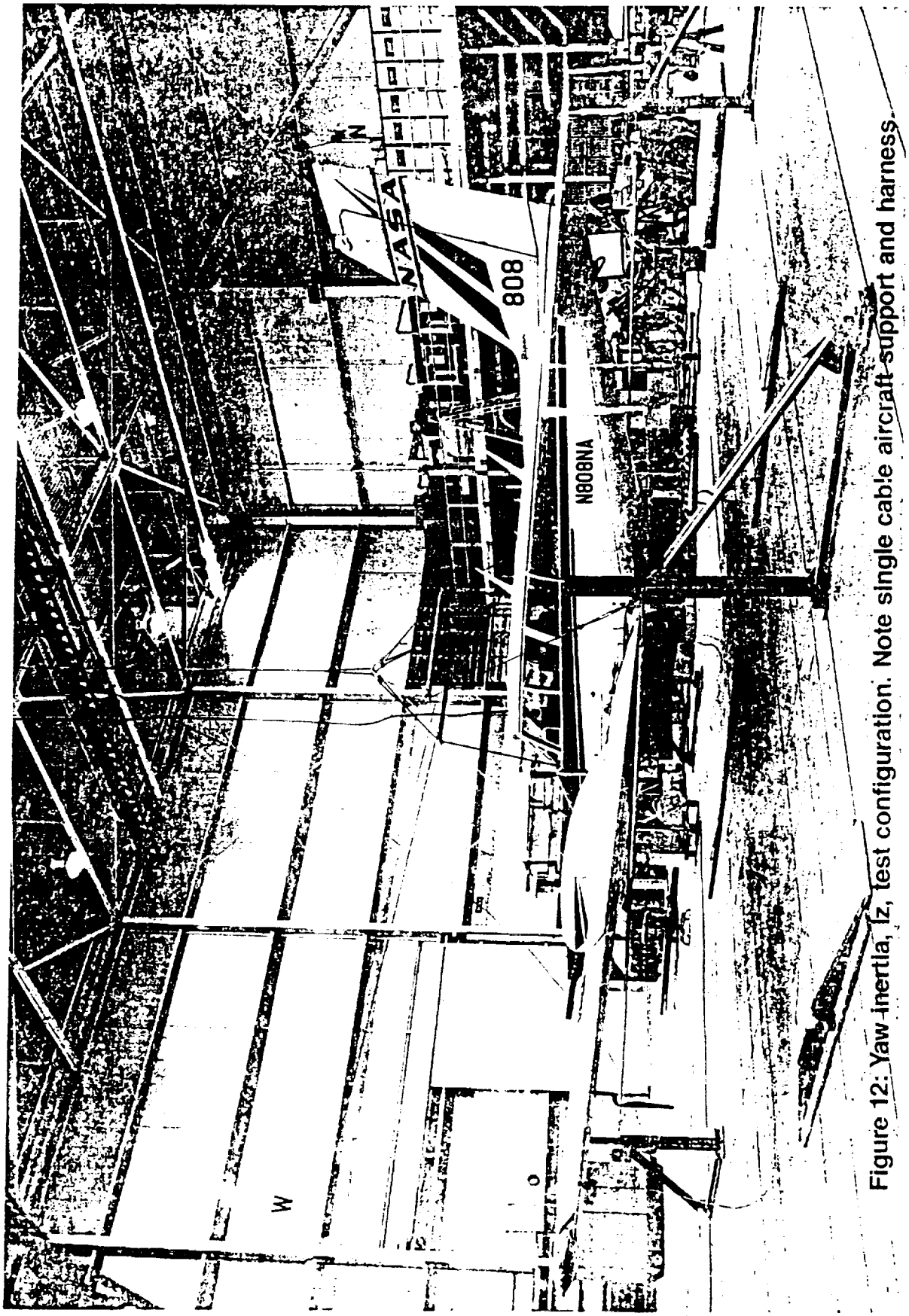

Figure 12: Yaw inertia, Iz, test configuration. Note single cable aircraft support and harness.

APPENDIXES

APPENDIX A

MMLE3 AIRCRAFT EQUATIONS OF MOTION

The following is a list of the equations of motion used in the computer program MMLE3, covered in detail in reference 5.

The longitudinal state, control, observation and extra signal vectors are

$$x = (\alpha \; q \; \theta)$$

$$u = (\delta_e)$$

$$z = (\alpha_m \; q_m \; \theta_m \; a_{n_m})$$

$$\text{extra} = (\bar{q} \; \beta \; p \; r \; \phi \; h \; V)$$

The nonlinear longitudinal state equations are

$$\dot{\alpha} = -\frac{\bar{q}S}{mV}(C_L + \alpha_o) + q + \frac{g}{V}(\cos\theta \cos\phi \cos\alpha + \sin\theta \sin\alpha) - \tan\beta\,(p\cos\alpha + r\sin\alpha)$$

$$I_y \dot{q} = \bar{q}\,Sc\,C_m + rp\,(I_z - I_x) + (r^2 - p^2)\,I_{xz}$$

$$\dot{\theta} = q\cos\phi - r\sin\phi + \dot{\theta}_o$$

The longitudinal observation equations are

$$\alpha_m = K\alpha\left(\alpha - \frac{X_\alpha}{V} q\right)$$

$$q_m = q$$

$$\theta_m = \theta$$

$$a_{n_m} = \frac{\bar{q}S}{mg} C_N + \frac{X_{a_n}}{g} \dot{q}$$

The expansions of the longitudinal force and moment coefficients are

$$C_m = C_{m_\alpha} \alpha + C_{m_q} \frac{qc}{2V} + C_{m_{\delta_e}} \delta_e + C_{m_o}$$

$$C_N = C_{N_\alpha} \alpha + C_{N_{\delta_e}} \delta_e + C_{N_o}$$

$$C_L = C_N$$

The approximation of $C_L = C_N$ is good for low angles of attack.

APPENDIX B

DETERMINATION OF MOMENTS OF INERTIA

The moments of inertia of the PA-30 were experimentally determined by the spring oscillation method. The moments of inertia (I_X, I_Y, I_Z) were determined for empty and full fuel conditions with no crew, and landing gear retracted. The vertical center of gravity position was also determined from these experiments.

Vertical CG

The vertical center of gravity was determined by the single-point suspension method (reference 7). In essence, this method applies known loads (F_a) to displace the suspended aircraft an angle (α) from a horizontal attitude. The following equation from reference 7 was used to determine the vertical CG position $\overline{Z}$ from the pivot support:

$$\overline{Z} = \frac{F_a}{W_s}\left(\frac{X_a}{\tan(\alpha)} + Z_a\right) \qquad \text{Eq. 1}$$

where Z_a is the vertical distance from the supporting pivot axis to the aircraft reference line (waterline zero). The parameters on the right side of the equation were measured directly from the test setup. The displaced angle, α, was measured with an inclinometer affixed to the aircraft. The test configuration is shown in figure 8. The weight W_s included all of the test equipment such as the cradle and supporting harness. The test equipment contributions were subtracted from the

experimental results. The vertical CG position was found to be about 4.33 inches below the aircraft's zero waterline reference.

Moments of Inertia

The moments of inertia were obtained experimentally by testing the aircraft and supporting cradle as a single unit. The equations used to solve for the moments of inertia were derived by summing the moments about p in the simple model of a spring weight system shown in figure 9. The applicable equation listed below was derived in reference 2 and is a general second order differential equation for damped harmonic motion.

$$\ddot{\theta} + \frac{c}{I_o}\dot{\theta} + \left(\frac{a^2k - Wh}{I_o}\right)\theta = 0 \qquad \text{Eq. 2}$$

where c is a viscous retarding moment and K is the spring constant.

Equation 2 is a linear differential equation with constant coefficients and is solved by the substitution method in reference 2. The solution of equation 2 is:

$$I_o = \frac{a^2k - Wh}{\omega_n^2} \qquad \text{Eq. 3}$$

where ω_n is the natural frequency of the system. The term I_o is the moment of inertia about the axis of rotation. The natural frequency was determined from the time history plots of angular velocity in the following manner. The damped frequency, ω_d, and the damping ratio, ξ, were computed as follows:

$$\omega_d = 2\pi f$$

$$\xi = \frac{\delta}{\sqrt{4\pi^2 + \delta^2}}$$

where f, the frequency of oscillation (cycles/second), is taken from the time history plots, and δ, the logarithmic decrement, is calculated using

$$\delta = \frac{1}{n} \ln \frac{x_o}{x_n}$$

with n the number of cycles and x the magnitude of the angular velocity recorded on the time history plots.

Then the natural frequency was determined using the equation below.

$$\omega_n = \frac{\omega_d}{(1 - \xi^2)^{1/2}}$$

The moment of inertia, about the rotation axes, I_o, was then transferred to the aircraft CG position using the parallel axis theorem to get I_{cg}.

$$I_{cg} = \frac{ka^2 - Wh}{\omega_n^2} - \frac{W}{g} d^2 - I_{te} \qquad \text{Eq. 4}$$

The equipment used in this test included the 256.5 pound supporting cradle, the springs, safety cables, and cradle harnesses. Anything that moved with the aircraft was taken into account. Only half the weight of items affixed to stationary supports was considered. Generally most items were small enough to consider their

moment of inertia about their own center of gravity to be zero. Thus the moment of inertia for test equipment, I_{te}, was simply

$$I_{te} = \frac{W_{te}}{g} (d_{te})^2$$

where W_{te} is the weight of the item and d_{te} is the distance from the center of gravity of the item to the oscillation axis.

The cradle's moment of inertia about its own CG, I_{cr}, was large enough to be considered, and was found by using the spring oscillation method

$$I_{te} \text{ (cradle)} = I_{cr} + \frac{W_{cradle}}{g} (d_{te})^2$$

Equation 4 is used for both the pitch and roll axis tests. The pitch test for I_y, pictured in figure 10, used one spring attached to the tail tiedown with the center of gravity of the aircraft located forward of the pivot point. The roll test for I_x, figure 11, used two springs affixed, one each, to the wing tiedowns and pivoted directly below the center of gravity position.

The single support cable, or pivot axis, for the yaw inertia test configuration, shown in figure 12, was directly above the center of gravity position of the aircraft so that the horizontal reference line was parallel to the floor and the single supporting cable coincided with the oscillation axis. This alignment results in zero values for distances d and h in equation 4. Thus the equation for yaw is

$$I_z = \frac{ka^2}{\omega_n^2} - I_{te}$$

The yaw inertia test used four springs horizontally attached with two at each wing tiedown point. The yaw analysis assumed the supporting cable to be free of torsional moments.

The spring oscillation method for determining the moments of inertia is relatively easy to use. However, many reference points exist for measuring distances. So it is a distinct advantage to simplify the procedure by recording all the vertical and horizontal distances to a reference point on the floor and knife edges.

The tests to determine the moments of inertia were made with the landing gear retracted at full and empty fuel conditions. This made it possible to interpolate the moments of inertia for different center of gravity positions. The moments of inertia are listed in Table 2.

REFERENCES

1. Maine, Richard E.; and Iliff, Kenneth W.; A Fortran Program for Determining Aircraft Stability and Control Derivatives from Flight Data. NASA TN D-7831, 1975.

2. Bradfield, Edward N.; Experimental Determination of the Moments of Inertia, Product of Inertia, and Inclination of the Principal Axis of Conventional Aircraft by the Spring Oscillation Method. Air Force Flight Test Center, June 1971.

3. Fink, Marvin P.; and Freeman, Delma C. Jr.; Full-Scale Wind-Tunnel Investigation of Static Longitudinal and Lateral Characteristics of a Light Twin-Engine Airplane. NASA TN D-4983, 1969.

4. Plaetschke, E.; and Schulz, G.; Practical Input Signal Design. AGARD Lecture Series No. 104 Parameter Identification.

5. Maine, Richard E.; and Iliff, Kenneth W.; Users Manual for MMLE3, A General Fortran Program for Maximum Likelihood Parameter Estimation. NASA Technical Paper 1563, 1980.

6. Iliff, Kenneth W.; and Taylor, Lawrence W. Jr.; Determination of Stability Derivatives from Flight Data Using a Newton-Raphson Minimization Technique. NASA TN D-6579, 1972.

7. Wolowicz, Chester H.; and Yancey, Roxanah B.; Experimental Determination of Airplane Mass and Inertial Characteristics. NASA TR R-433, 1974.